

1 Deciphering the enigmatic origin of Guyana's diamonds. (Revision 2)

2 Roy Bassoo^{1*}, Kenneth S. Befus¹, Peng Liang¹, Steven L. Forman¹, Glenn Sharman²

3 Key Words: diamond, Guyana, Guiana Shield, Roraima Supergroup.

4 **Abstract**

5 Diamonds have long been mined from alluvial terrace deposits within the rainforest of Guyana,
6 South America. No primary kimberlite deposits have been discovered in Guyana, nor has there
7 been previous studies on the mineralogy and origin of the diamonds. Paleoproterozoic terranes in
8 Guyana are prospective to diamond occurrences because the most productive deposits are
9 associated spatially with the eastern escarpment of the Paleoproterozoic Roraima Supergroup.
10 Geographic proximity suggests that the diamonds are detrital grains eroding from the <1.98 Ga
11 conglomerates, metamorphosed to zeolite and greenschist facies. The provenance and
12 paragenesis of the alluvial diamonds are described using a suite of placer diamonds from
13 different locations across the Guiana Shield. Guyanese diamonds are typically small, and those
14 in our collection range from 0.3 to 2.7 mm in diameter; octahedral and dodecahedral, with lesser
15 cubic and minor macle forms. The diamonds are further subdivided into those with abraded and
16 non-abraded surfaces. Abraded diamonds show various colors in cathodoluminescence whereas
17 most non-abraded diamonds appear blue. In all populations, diamonds are predominantly
18 colorless, with lesser brown to yellow and very rare white. Diamonds are predominantly Type
19 IaAB and preserve moderate nitrogen aggregation and total nitrogen concentrations ranging from
20 trace to ~1971 ppm. The kinetics of nitrogen aggregation indicate mantle-derived residence
21 temperatures of 1124 ± 100 °C, assuming residence times of 1.3 Ga and 2.6 Ga for abraded and
22 non-abraded diamonds respectively. The diamonds are largely sourced from the peridotitic to

¹ Baylor University, Department of Geosciences. One Bear Place, #97354, Waco, Texas, USA, 76798.
Roy_Bassoo1@Baylor.edu (*corresponding author)

² University of Arkansas, Department of Geosciences. 340 N. Campus Dr., Fayetteville, Arkansas, USA, 72701.

23 eclogitic lithospheric upper mantle based on both $\delta^{13}\text{C}$ values of $-5.82 \pm 2.45\%$ (VPDB-LSVEC)
24 and inclusion suites predominantly comprised of forsterite, enstatite, Cr-pyrope, chromite, rutile,
25 clinopyroxene, coesite, and almandine garnet. Detrital, accessory minerals are non-kimberlitic.
26 Detrital zircon geochronology indicates diamondiferous deposits are predominantly sourced
27 from Paleoproterozoic rocks of 2079 ± 88 Ma.

28 **Introduction**

29 Diamonds have been mined for the past century from alluvial gravels along the rivers and
30 creeks deep within Guyana's Amazon rainforest. The diamonds are found as placers in paleo-to-
31 modern channels, terraces, and streambeds. Guyana's diamonds are found in headless placers,
32 with the most productive gravels associated spatially with the eastern escarpment of the Roraima
33 Supergroup, which suggests that the diamonds originate from this detrital source (Fig. 1). The
34 humid tropical climate and ancient weathering profile of the Guiana Shield makes addressing
35 diamond provenance a difficult task. Exploration has been driven by artisanal miners who
36 prospect using detrital indicator minerals. No primary kimberlites are known in the region, and
37 there is a lack of prior research on the nature and origin of diamonds in Guyana (e.g., Gibbs and
38 Barron 1993, Shields and Letendre 1999, Persaud 2010).

39 Several hypotheses exist on the origin of Guyana's diamonds. Diamonds may be sourced
40 from yet undiscovered primary kimberlites or igneous intrusions (Shields and Letendre 1999;
41 Persaud 2010). The most likely location would be associated spatially with the highly magnesian
42 ultramafic intrusives of the 1.7 ± 0.2 Ga, Badidku suite (Olszewski et al. 1977). These rocks
43 intruded during a tectonically quiet period of the late Trans-Amazonian orogeny (Gibbs and
44 Barron 1999) and might be associated with other ultramafic intrusions such as kimberlites. The
45 only confirmed examples of primary diamond deposits in the Guiana Shield are in Guaniamo,

46 Venezuela, and Dachine, French Guiana (Fig. 1), where diamonds are found in Neoproterozoic
47 kimberlite sills and metamorphosed Paleoproterozoic ultramafic and pyroclastic shoshonites or
48 lamprophyres, respectively (Capdevila et al. 1999; Magee and Taylor 1999; Kaminsky et al.
49 2000; Channer et al. 2001; Kaminsky et al. 2004; Wyman et al. 2008; Smith et al. 2016).
50 Kimberlites exist in Roraima, Brazil, but these are not diamondiferous (Svisero et al. 2017,
51 Cabral et al. 2017). Known diamondiferous kimberlites from West Central Africa are an
52 additional potential source for Guyana's alluvial deposits (Reid 1974 and Briceno 1984). These
53 regions were immediately adjacent prior to the Jurassic rifting and opening of the Atlantic
54 Ocean; separated by 200 to 400 km (Fig. 1). If diamonds were derived from Africa then they
55 would be more prevalent in the northeastern Guiana Shield where diamonds are not found.
56 Furthermore, West African diamonds have been traced to the host diamondiferous kimberlites
57 which range in age from 92 – 846 Ma (Bardet and Vachette 1966; Andrews-Jones 1968; Hall
58 1972; Janse 1996; Fourie et al. 1998; Fourie et al. 2000; Kiviets 2003; Skinner et al. 2004). More
59 locally, the Avanavero mafic dykes and sills (<1.79 Ga) have been suggested to be
60 diamondiferous, but these dykes are tholeiitic norites and gabbros and thus unlikely to be
61 diamond-bearing (Da Silva Rodrigues 1991; Reis et al. 2000; Heesterman et al. 2005). Finally,
62 the diamonds may be derived as detrital grains weathering directly from diamondiferous
63 conglomerates of the Paleoproterozoic Roraima Supergroup (e.g., Gibbs and Barron 1993;
64 Meyer and McCallum 1993). This may be plausible because alluvial diamonds are sometimes
65 found in gravels with abundant, rounded quartz, red jasper, and quartzite clasts; also observed in
66 Roraima Supergroup conglomerates. Placer diamonds in Mutum, Brazil are mined from alluvial
67 terraces shed possibly from conglomerates of the Tepequém Formation, which is equivalent to
68 the Arai Formation pebbly sandstones and volcanoclastics of the Roraima Supergroup (Santos et

69 al. 2003; Reis et al. 2017). Similarly, in Suriname, diamonds are found in alluvium shed from
70 metamorphosed Proterozoic conglomerates or ultramafic volcanoclastics of the Rosebel group,
71 but their provenance remains unknown (van Kooten 1954; Schönberger and de Roeve 1974;
72 Schönberger 1975; Bosma et al. 1983; Ramlal 2018; Naipal et al. 2019). The Roraima
73 Supergroup and similar sedimentary sequences may have been a sink for diamonds erupted by
74 unknown Paleoproterozoic kimberlites, and may be detrital evidence for some of Earth's earliest
75 kimberlites.

76 Guyana's diamonds are a known commodity in the global diamond trade, referred to as
77 "British diamonds," stemming from a colonial past. Economically valuable diamonds in Guyana
78 are small, most commonly ranging from 0.1 to 0.4 carats although larger stones are found.
79 Guyanese diamonds are predominantly colorless (G-J), yellow (K-M), and brown. Pink and
80 green body colors are rare. Exploration activities conducted by Golden Star resources recovered
81 alluvial diamonds and accessory minerals from Amatuk (Fig. 1) and are described as octahedral
82 with moderate resorption textures. Green and brown spotting and skins are attributed to radiation
83 damage from accessory zircon, monazite, uraninite, micas, and K-feldspar (Breeding et al. 2018),
84 when residing in a placer environment. Surface abrasion and breakage post-dating resorption
85 along crystal edges were interpreted to be derived from either a high energy fluvial environment
86 or agitation during recovery (Shields and Letendre 1999).

87 We present the morphology, abrasion and dissolution textures, nitrogen concentration,
88 carbon isotopic composition, and inclusion mineralogy of Guyana's alluvial diamonds to learn
89 about their provenance, host magma characteristics, residence temperatures, and mantle source
90 beneath the Guiana Shield. We characterize Guyana's diamonds and their accessory minerals,
91 thereby facilitating meaningful comparisons with other diamond deposits in the Guiana Shield

92 and elsewhere. Diamonds were obtained from the Ekereku, Jawalla, Konawaruk, Kamarang,
93 Kurupung, Maikwak, and Monkey Mountain alluvial deposits in Guyana (Fig. 1). Most
94 diamonds crystallized from peridotitic lithosphere, although there is a lesser population of
95 eclogitic diamonds. These diamonds can be divided into two basic groups; those with and
96 without sedimentological abrasive textures. Importantly, non-abraded and abraded diamonds
97 have statistically different cathodoluminescence, ultraviolet blue light luminescence, and Fourier
98 Transform Infrared (FTIR) responses. Abraded diamonds are evidence for a detrital, polycyclic
99 source weathering from the Roraima Supergroup. Non-abraded diamonds may be derived from
100 the Roraima Supergroup, but have experienced less transport and recycling.

101 **Regional Geology**

102 Diamonds occur across the Guiana Shield and lesser portions of the Guaporé Shield
103 within the Amazonian craton of South America (Fig. 1). The Guiana Shield is exposed for over
104 900,000 km² along the northern margin of the Amazonian Craton. Chemical weathering prevails
105 throughout much of the Guiana Shield, resulting in thick sequences of saprolite capped by “tor”
106 formations of large boulders of resistive and residual host rock, with the saprolite regolith
107 stripped away by weathering (Kroonenberg and Gersie 2019). Although exposures are limited by
108 accessibility and extreme tropical weathering, there is broad consensus that the Paleoproterozoic
109 evolution of this craton was dominated by episodes of accretionary orogenic events around an
110 Archean core complex during the Main Trans-Amazonian (2.26-2.08 Ga) to Late Trans-
111 Amazonian (2.07-1.93 Ga) orogenies (Tassinari 1997; Vanderhaeghe et al. 1998; Reis et al.
112 2000; Delor et al. 2003; Cordani and Teixeira 2007; Fraga et al. 2009; Daoust et al. 2011;
113 Kroonenberg et al. 2016).

114 The Guiana Shield is divided into four major Paleoproterozoic terranes (Daoust et al.
115 2011), one Mesoproterozoic terrane, and two isolated Archean terranes (Norcross 1997;
116 Kroonenberg et al. 2016). Crustal development in the Guiana Shield created a series of
117 greenstone belts, associated gneisses, and amphibolites of the Maroni-Itacaiunas Belt (Tassinari
118 et al. 1997). The greenstone belts underwent several episodes of deformation, intrusion, and
119 metamorphism between 2.26 Ga and 2.08 Ga, followed by cooling between 2.08 Ga and 1.93
120 Ga. These events are interpreted to reflect the expression of the Trans-Amazonian Orogeny in
121 the Guiana Shield (Cordani and De Brito Neves 1982; Gibbs and Barron 1993; Norcross 1997;
122 Daoust et al. 2011). Much of the region was then unconformably overlain by the Roraima
123 Supergroup, which is a stratigraphic succession dominated by interbedded 1.98 - 1.78 Ga
124 sandstones and conglomerates deposited from rocks eroding from earlier greenstone terranes
125 (Priem et al. 1973; Santos et al. 2003). Finally, coeval mafic dykes of the Avanavero Suite
126 intruded the entire sequence at ~1.79 Ga (Reis et al. 2000).

127 The region has been a stable craton, only modified by erosional processes, throughout
128 much of the late Phanerozoic. The upper Proterozoic was marked by a period of prolonged uplift
129 with no evidence of sedimentation (Gibbs and Barron 1993). Changing climate and repeated
130 uplift cycles since the late Triassic have resulted in continuing surface evolution of the Guiana
131 Shield. Rifting of South America from Africa beginning in the early Jurassic was associated with
132 accelerated weathering and fluvial activity (McConnell 1968). The regional drainage patterns
133 and depositional systems have evolved in response to millions of years of river capture,
134 rejuvenation, degradation, and aggradation initiated by faulting and rifting since the opening of
135 the Atlantic Ocean. Today the region preserves a complex network of high alluvial, terrace,
136 alluvial flat, river bed, buried channel, and plateau deposits. Repeated cycles of erosion and

137 deposition have led to complex diamond placer deposits with detrital assemblages reflecting
138 variable provenance and timing. The diamonds are found alongside accessory phases that include
139 quartz, topaz, jasper, rutile, anatase, zircon, ilmenite, gold, corundum, and tourmaline, with
140 minor garnet and chromite. Olivine and perovskite are notably absent. Diamond is the only
141 residual mineral that certainly eroded from kimberlite rock. Despite the possibility for primary
142 kimberlite sources and the complex geologic history of the Guiana Shield, placer deposits are the
143 only diamond sources that have been discovered in Guyana.

144 **Methods**

145 We acquired a collection of diamonds from miners and a local diamond merchant (Kay's
146 Diamond Enterprise Ltd.). We first cataloged each stone by measuring its dimensions and mass.
147 The overall morphology of the diamonds was then assessed using a Zeiss Scope AX IO
148 petrographic microscope. A focus was delineating crystal shape, dissolution textures, and
149 abrasion. Some features were documented using high resolution scanning electron microscopy
150 energy dispersive X-ray (SEM-EDS) spectroscopy at the Baylor University Center for
151 Microscopy and Imaging.

152 The nitrogen content of 415 diamonds were measured, and the aggregation state
153 calculated for the majority of samples using a Thermoscientific Nicolet iN10 FTIR spectrometer.
154 Analyses were performed across $675\text{-}4000\text{ cm}^{-1}$ in cooled transmission mode using a 200×200
155 μm aperture size, 64 scans, and spectral resolution of 4 cm^{-1} . Nitrogen concentration was
156 calculated from individual spectra by applying the Beer-Lambert law and absorption values of
157 nitrogen bands at 1365 , 1284 , and 1175 cm^{-1} , using the least-squares fitting approach (e.g.,
158 Howell et al. 2012).

159 Effective thickness (x) was calculated by normalizing the absorption coefficient (μ) of
160 diamond lattice bands at 2443, 2158, and 2026 cm^{-1} , where $x = \mu_{2443}/5$; $x = \mu_{2158}/12$; $x = \mu_{2026}/12$
161 and the average effective thickness was then calculated (Kaminsky and Khachatryan 2012).
162 Stable carbon isotope analyses ($\delta^{13}\text{C}$, in ‰_{VPDB-LSVEC}) were performed at the Baylor University
163 Stable Isotope Laboratory using a Costech Elemental Combustion System 4010 connected to a
164 Thermo-Electron Delta V Advantage continuous flow Isotope Ratio Mass Spectrometer (CF-
165 IRMS) through a Thermo Conflo IV interface. Fifty-seven crushed and powdered diamond
166 samples (<0.5mm) which range from 0.05 – 0.90 mg (mean - 0.26 ±0.15 mg) were loaded into
167 silver capsules, flash combusted at 1000°C to convert the diamond to CO_2 , which was carried to
168 the CF-IRMS by a constant helium gas flow.

169 Optical cathodoluminescence (CL) of 556 diamonds was observed using a Nikon-Japan
170 LV UEPI microscope equipped with a low vacuum Reliotron III that operated at 7.5-9 kV and
171 0.3-0.5 amps. The CL data was supplemented with ultraviolet blue light (UV) luminescence
172 (425-495 nm) observed in 558 diamonds using an Olympus BX51 petrographic microscope
173 equipped with an EXFO X-cite 120 fluorescence illumination system, with an exposure time of
174 approximately 10 s for most samples. Each crystal's color, or lack thereof, was documented for
175 both CL and UV observations.

176 Inclusions within 91 diamonds were identified using Raman spectra collected with a
177 ThermoScientific DXR Raman microscope equipped with a 532 nm laser operating at 8 mW, a
178 ~2- μm spot, and a high resolution 1800 lines mm^{-1} grating. Inclusion species were identified by
179 matching diagnostic peak positions and heights of unknown spectra with those in the RRUFF
180 spectral database (Lafuente et al. 2016).

181 Accessory minerals were extracted from heavy mineral separates that we collected from
182 buried alluvial and colluvial deposits in the Kurupung region (UTM WGS 84 Zone 20N,
183 804678E, 675615N), approximately 4km from the base of the Roraima Supergroup escarpment.
184 Rare diamonds were also recovered from these heavy mineral separates. Samples were sieved,
185 separated by mass in a shaker table, and cleaned in a sonic bath. Hand-picked accessory minerals
186 of garnet, chromite, and ilmenite were mounted in epoxy, polished at Baylor University and
187 analyzed at the University of Texas at Austin, using a JEOL JXA-8200 Electron Microprobe
188 (EPMA). Zircon crystals were also handpicked and analyzed for U-Pb crystallization ages using
189 laser-ablation-inductively coupled plasma-mass spectrometry (LA-ICPMS) at the University of
190 Arkansas Trace Element and Radiogenic Isotope Laboratory. For each sample, 150 detrital
191 zircon grains were mounted on a glass slide using double-sided tape. Grain surfaces were ablated
192 using an ESI 193 nm Excimer laser ablation system and a Thermo iCap quadrupole ICP-MS.
193 Data acquisition parameters include a 35 μm spot size, laser repetition rate of 10Hz, helium flow
194 rate of 0.8 L min⁻¹, and a fluence of $\sim 4.5 \text{ J cm}^{-2}$. Zircon from Plesovice (337.13 Ma; Slama et al.,
195 2008) was used as a primary standard, with R33 (419 Ma; Black et al., 2004) as a secondary
196 standard. The weighted mean average of R33 analyses was within 1% of the accepted age. Data
197 were reduced in Iolite v. 3.71 (Paton et al., 2011), and individual analyses were manually
198 trimmed to avoid zones of high discordance and ²⁰⁴Pb bearing inclusions. Twenty-four analyses
199 were excluded because they were not zircon or were contaminated by inclusions. An additional
200 17 zircon grains (5.6% of the total) were excluded on the basis of discordance (²⁰⁷Pb/²⁰⁶Pb versus
201 ²⁰⁶Pb/²³⁸U) exceeded 10% or 5% reverse discordance. In total, 259 concordant zircon U-Pb
202 analyses were retained (Fig. A1; Table A5).

203 Results

204 **Morphology**

205 Diamonds in our collection range in size from 0.3 to 2.7 mm in diameter; with a mean of
206 1.1 ± 0.2 mm. Masses range from 0.01 g to 0.95 g. Diamonds are predominantly colorless (93%)
207 with lesser amounts of brown (4%) to yellow (3%) and very rare white (1%) variants (Fig. 2).
208 Approximately half of the diamonds show no radiation spotting (55%). The remainder has green
209 to green-blue skins or green spotting that covers up to ~100% of the surface area. A small
210 population (5%) show combined overprinting of brown and green spotting (Table 1).

211 Diamonds across all regions are octahedral (30%) and dodecahedral (30%), with lesser
212 combination (16%), flattened or elongate (15%), and cubic (3%) forms (Fig. 3) (Table 1). Those
213 from Ekereku present more dodecahedrons (46%) than octahedrons (31%). Kamarang has the
214 most flattened or elongated diamonds (26%), with the remainder being octahedral, dodecahedral,
215 and various combinations. Twinned diamonds and aggregates are rare from any location.
216 Fragments account for 9% of diamonds analyzed and resorbed fracture or fragmented diamond
217 surfaces were not observed.

218 Fine stepwise, lamellar trigonal faces are common, whereas flat faces and sharp edges are
219 uncommon (Fig. 3). Resorption textures, including terraces, tear drop hillocks, and dissolution
220 pits are common in 95% of diamonds. Most octahedral diamonds have resorbed edges, and in the
221 case of Ekereku, more diamonds are fully resorbed to dodecahedrons. Tear drop hillocks are the
222 most common dissolution texture (Fig. 3f). The most common pit dissolution textures are flat
223 bottom (37%) and point bottom (12%) trigons and tetragons (19%) (Table 2). Very fine (8%) to
224 fine (3%) point bottom trigons are more abundant than coarse to very coarse point bottom
225 trigons. Very fine (5%) to fine (14%) flat bottom trigons are slightly more abundant than coarse
226 (12%) to very coarse (1%) flat bottom trigons. Point bottom hexagons, and trapezoids are

227 notably rare. Late stage etching features such as corrosion sculptures, shallow depressions, ruts,
228 and glossy surfaces are observed in two-thirds of the diamonds. Less than 5% of diamonds show
229 fine to medium microdisc textures, but when present occur in swarms.

230 Edge abrasion is found in 44% of abraded diamonds and is the most common
231 sedimentologic-induced surface texture (Fig. 3i). Percussive marks along crystal edges,
232 scratches, and crescentiform fissures are less common (Fig. 3j). Most diamonds have some
233 degree of surface abrasion from minor scratches and edge abrasion and some have no apparent
234 surface abrasion. This distinction in surface texture is the basis to subdivide Guyana's diamonds
235 into abraded (85%) and non-abraded (15%) populations. Abraded diamonds may reflect an older
236 population with extensive fluvial communitation, whereas, the non-abraded diamond population
237 may reveal a shorter distance and/or time of fluvial transport. Ekereku has the highest relative
238 proportion of non-abraded diamonds followed by Kamarang and Kurupung, whereas Jawalla,
239 Konawaruk, Monkey Mt., and Maikwak, have no abraded diamonds. Abraded diamonds average
240 mass (9.3 ± 21.5 mg) is larger than that of non-abraded diamonds (5.5 ± 4.2 mg). Non-abraded
241 diamonds are more dodecahedral in form (45% compared to 25%) (Table A1). Resorbed abraded
242 diamonds present more flat-bottomed dissolution textures (85.3%) than point-bottom dissolution
243 textures (18.7%). Non-abraded diamonds also present greater flat-bottomed dissolution textures
244 (56.5%) than point-bottom dissolution textures (43.5%), but to a lesser degree (Table A1).

245 **Cathodoluminescence and UV luminescence**

246 Guyana's diamonds cathodoluminesce green (35%), blue (25%), and turquoise (18%)
247 with lesser orange, red, and yellow (Table 3). Abraded and non-abraded diamonds demonstrate
248 different responses to CL. Guyana's abraded diamonds dominantly show green CL (39%),
249 turquoise (19%), and blue (19%), with minor orange, red, and yellow (~10%), with 11% non-

250 luminescent (Fig. 4a). In contrast, non-abraded diamonds cathodoluminesce blue (59%), minor
251 green (13%), turquoise (10%), and orange (4%), with 13% showing no CL. No yellow or
252 combination CL was observed. Statistical analyses (χ^2 tests) demonstrate with >99% certainty
253 that the frequencies of CL response between abraded and non-abraded diamonds are independent
254 (Table 4).

255 Ultraviolet luminescence also yields a clear distinction between abraded and non-abraded
256 diamonds. Abraded diamonds UV luminesce green (84%) with very minor orange (1%), red
257 (2%), and yellow (3%) variants, and 10% with no apparent luminescence. In contrast, non-
258 abraded diamonds show a smaller population of green-luminescent grains (52%), and minor
259 populations of red- (1%) and yellow-luminescent (1%) grains. A large proportion of non-abraded
260 diamonds yielded no luminescence response (45%) (Fig. 4b). We note that similar CL and UV
261 response distributions are observed for all diamonds regardless of geographic location.

262 **Nitrogen and Carbon isotope composition**

263 The nitrogen concentration of diamonds range between trace (< 5 ppm ~ Type IIa) and
264 1971 ppm, with a mean of 315 ± 24 ppm and rare outliers from 1175 to 1971 ppm. Diamonds are
265 predominantly Type IaAB, accounting for 53%, with Type IaA at 22%, and Type IaB at 9%.
266 17% of the diamonds are Type IIa and thus show no nitrogen aggregation (Fig. 5). No Type IIb
267 diamonds are observed.

268 Marked differences in nitrogen concentration exist between abraded and non-abraded
269 diamonds (Table 4). Non-abraded diamonds have higher average nitrogen concentrations
270 compared to abraded diamonds with means of 621 ± 47 ppm and 271 ± 21 ppm, respectively
271 (Fig. 5; Table 4). The nitrogen concentrations of non-abraded diamonds preserve a more uniform
272 distribution with lower skewness and kurtosis coefficients of 0.26 and 1.91, whereas the abraded

273 diamonds display a pronounced positive skewness (1.82) and a higher kurtosis (6.62) (Table 4;
274 Fig. A1). Multivariate density Finite Mixture Modeling of nitrogen concentrations was applied to
275 determine if subpopulations could be readily identified within the greater abraded and non-
276 abraded diamond populations, based on the Bayesian Information Criteria which demonstrates
277 that a 21 component mixture is the most appropriate choice (Fig. A2) (e.g., Schwartz, 1978;
278 Galbraith and Green 1990; Liang and Forman 2019; McLachlan et al. 2019). The Finite Mixture
279 Modeling identified ten distinct subpopulations within the abraded diamonds and seven
280 subpopulations within the non-abraded diamonds (Table 4). The abraded and non-abraded
281 diamonds may share six subpopulations, with nitrogen concentrations of 604 ± 48 , 390 ± 48 , 180
282 ± 16 , 47 ± 3 , 23 ± 1 , and 4 ± 0.3 ppm. The non-abraded population may have one additional
283 group centered at 968 ± 79 ppm, whereas the abraded diamonds may have additional populations
284 at 13 ± 1 , 84 ± 8 , 1234 ± 99 , and 1911 ± 150 ppm. Nitrogen concentrations reported here are
285 average and bulk compositions intended to characterize the diamond populations as a whole.
286 Heterogeneity within each individual diamond is expected but not elaborated further.

287 Guyanese diamonds have an average $\delta^{13}\text{C}$ value of $-5.82 \pm 2.45\text{‰}$ with a range from -
288 16.11 to -2.88‰ . These $\delta^{13}\text{C}$ values are slightly more depleted than diamonds from Arenápolis
289 and Boa Vista, Brazil, and are significantly more enriched in ^{13}C than those of Guaniamo,
290 Venezuela ($-15 \pm 2.78\text{‰}$), and Dachine, French Guiana ($-24.65 \pm 4.12\text{‰}$) (Fig. 6). Diamonds
291 from West and Central Africa preserve a mode of -3.5‰ , making them more enriched than
292 Guyana's diamonds (Cartigny et al. 2014). Abraded diamonds have an average $\delta^{13}\text{C}$ value of -
293 $6.11 \pm 2.71\text{‰}$ and non-abraded diamonds have an average $\delta^{13}\text{C}$ value of $-5.06 \pm 1.36\text{‰}$. For
294 comparative spectroscopy, luminescence, $\delta^{13}\text{C}$, morphology, and inclusion paragenesis of
295 Guyana's diamonds please see supplementary Tables A1-A4.

296 **Inclusions**

297 Diamond-hosted inclusions in order of decreasing abundance include forsteritic olivine,
298 enstatitic orthopyroxene, rutile, chromite, garnet, clinopyroxene, and coesite (Table 5).
299 Epigenetic inclusions consist of graphite, which are restricted to internal fractures within the
300 diamond or along relaxed inclusion margins. Sulfide inclusions are rare. Most primary inclusions
301 of olivine and orthopyroxene are cubo-octahedral, whereas clinopyroxene are prismatic to
302 elongate cubo-octahedral. Forsteritic olivine is the most common inclusion, found in 6.3% of all
303 diamonds examined. When found, olivine occurs as single inclusions or in clusters. Olivine
304 inclusions are colorless and range in size from ~ 5 to 500 μm . Orthopyroxene is found in 2.3% of
305 diamonds. It is colorless and inclusions are ~ 5 to 550 μm across. Garnet inclusions occur in
306 0.6% of diamonds. Garnets range in size from ~ 25 to 200 μm . Three garnets are purple and one
307 is red-brown.

308 **Accessory mineral geochemistry**

309 Guyana's alluvial diamond deposits are frequently found with non-
310 kimberlite water worn quartz, topaz, jasper, rutile, anatase, zircon, ilmenite, gold, corundum, and
311 tourmaline, with minor garnet and chromite. Traditional kimberlite indicator minerals are
312 uncommon but chromite, garnet, and ilmenite occur in our samples (Table A4). Two populations
313 of mantle derived and crustal derived garnets are observed based on discrimination diagrams of
314 Schulze et al. 2003 (Fig. 7). Crustal garnets are Mn-rich spessartines ($\text{Alm}_{27\pm 19}\text{Py}_{2\pm 5}\text{Sp}_{70\pm 23}$). The
315 mantle derived garnets ($\text{Alm}_{3\pm 3}\text{Py}_{12\pm 2}\text{Sp}_{84\pm 3}$) are also low Cr and have moderately low TiO_2 (~
316 0.19 wt%). SEM-EDS profiles of both garnet populations show no obvious compositional zoning
317 or evidence of metamorphic overprint. Accessory ilmenite grains are MgO poor (0.17 ± 0.4
318 wt%) and TiO_2 rich ulvospinel (72.2 ± 7.6 wt%) ($\text{Wu}_{72\pm 16}\text{Ru}_{28\pm 16}$). We analyzed chromite in our

319 samples and compared them to previous analyses of accessory chromite conducted by Goldenstar
320 resources from diamondiferous alluvial deposits in Amatuk (Shields and Letendre 1999). Most
321 chromites have moderate to low TiO_2 (0.5 ± 0.8 wt%) and Al_2O_3 (14.2 ± 5.6 wt%) demonstrating
322 magmatic arc (ARC) and mid ocean ridge basalt (MORB) affinities.

323 **Detrital zircon geochronology**

324 Two representative diamond-bearing heavy mineral separates from the Kurupung region
325 were targeted for reconnaissance detrital zircon geochronology. The first was from colluvium in
326 a raised terrace, approximately 3 m above the modern river (KU002). The second was collected
327 from an alluvial gravel horizon within a buried fluvial channel. Most zircons are well rounded by
328 abrasion. A minor proportion ($\sim 8\%$) of zircons occur as slightly abraded to non-abraded
329 euhedral, doubly terminated prisms. Detrital zircon age distributions of both buried alluvium and
330 terrace colluvium samples are dominated by zircon between 2.0 and 2.2 Ga in age; recording
331 similar peak ages of 2.06 Ga and 2.04 Ga, respectively (Fig. A2). Only 5 grains of earliest
332 Paleoproterozoic or Archean in age (i.e., > 2.3 Ga) were identified ($\sim 2\%$ of the total), and these
333 grains are generally late Archean (2.6-2.8 Ga) (Fig. 8). All zircon U-Pb analyses are older than
334 the depositional age range of the 1.78 ± 0.03 Ga – 1.98 ± 0.08 Ga Roraima Supergroup (Santos
335 et al. 2003).

336 **Discussion**

337 Guyana's alluvial diamond deposits represent an economic resource that also preserve
338 valuable insights into the evolution of surface and subsurface processes of the Guiana Shield.
339 Hypotheses regarding the mantle paragenesis and surface provenance of Guyana's diamonds
340 exist, but each are based largely on speculation. Our morphology, composition, and inclusion

341 datasets provide empirical based reasoning to characterize the mantle conditions of diamond
342 formation and identify the possible provenance of placer alluvial deposits.

343 The Guiana Shield has existed as a thick craton with lithospheric roots extending >130
344 km depth since at least 1.9 Ga (Gibbs and Barron 1993; Schulze et al. 2006). Such depths are
345 enough to intersect the diamond stability field beneath the craton (Stachel and Harris 2009),
346 depending on the thermal regime during that time. However, kimberlite deposits in Guyana have
347 not been discovered, unlike elsewhere in the Guiana Shield (Kaminsky et al. 2000; Channer et al.
348 2001; Kaminsky et al. 2004; Svisero et al. 2017, Cabral et al. 2017). Instead, diamonds are
349 recovered from Quaternary to modern alluvial deposits. Tectonic and sedimentologic processes
350 may have mixed diamonds from different temporal and geographic sources into the same alluvial
351 basins. Thus, Guyana's diamonds reflect complex surface and mantle processes across the
352 Guiana Shield, since the Paleoproterozoic.

353 **Paragenesis**

354 Diamonds preserve both compositional and physical evidence of their parental mantle
355 source. During crystal growth, diamonds may entrap particular suites of minerals as inclusions.
356 Guyanese diamonds primarily contain inclusions of forsteritic olivine, enstatitic orthopyroxene,
357 and chromite. This assemblage indicates most of the diamonds crystallized in, and were
358 extracted from, the harzburgite peridotite dominated upper mantle. Less common diamonds
359 preserve an eclogitic assemblage containing rutile, almandine garnet, clinopyroxene, and coesite
360 inclusions. Cratonic lithospheric mantle assemblages are typically stable between 1 and 7 GPa
361 and less than 1300°C (Mather et al. 2011). Both peridotite and eclogite assemblages spatially
362 coexist beneath stable cratons, consistent with model geothermal gradients of 38-42 mWm⁻²
363 (Pollack and Chapman 1977; Stachel and Harris 2009).

364 The carbon isotopic composition of diamonds can be used to further resolve mantle
365 paragenesis. Guyana's diamonds yield an average $\delta^{13}\text{C}$ value of $-5.82 \pm 2.45\text{‰}$ (Fig. 6), falling
366 within the range of -8 to -2‰ found in most P-type diamonds sampled from the peridotitic upper
367 mantle (Cartigny 2005). Few diamonds have values less than -10‰. These light $\delta^{13}\text{C}$ values are
368 E-type, having crystallized from eclogite and contain a possible organic carbon source derived
369 from metasedimentary rocks (Cartigny et al. 2014). Very light $\delta^{13}\text{C}$ values ($< -16\text{‰}$) might be
370 indicative of websteritic paragenesis (Deines and Harris 2004) but are rare in Guyana's
371 diamonds. Together, Guyana's diamond inclusion suites and carbon isotopic compositions
372 confirm that the diamonds are largely sourced from the lithospheric mantle and derived from
373 predominantly peridotite and eclogite rocks.

374 Accessory mineral compositions can also be used to infer the paragenesis of Guyana's
375 diamond deposits. Accessory garnet is spessartine ($\text{Alm}_{27\pm 19}\text{Py}_{2\pm 5}\text{Sp}_{70\pm 23}$) in composition and
376 most are likely derived from granite and granodiorite rocks, which are common throughout the
377 Guiana Shield. A subpopulation of the spessartine preserves Mg/Ca ratios indicative of a mantle
378 derived affinity (Fig. 7; $\text{Mg}\#/\text{Ca}\# \sim 3.80$). These mantle spessartines ($\text{Alm}_{3\pm 3}\text{Py}_{12\pm 2}\text{Sp}_{84\pm 3}$) have
379 low Cr and low TiO_2 concentrations and are likely derived from eclogitic source rocks (Schulze
380 et al. 2003). Although sourced from the mantle, these garnets are not likely of kimberlitic origin.
381 Instead, these low-Cr and low- TiO_2 spessartine were more likely derived from subducted oceanic
382 crust rich in Mn. In Guyana there are early Proterozoic manganeseiferous metasedimentary rocks
383 (Gibbs and Barron 1993); the largest of which are at Mathews Ridge which outcrops north of the
384 Roraima Supergroup (Westerman 1969). These could be remnants of subducted oceanic crust
385 from which the mantle affiliated garnets are derived. Accessory ulvospinel ($\text{Wu}_{72\pm 16}\text{Ru}_{28\pm 16}$) are
386 Mg-poor and are similarly derived from non-kimberlite mafic intrusions. Most chromites have

387 moderate to low TiO_2 and Al_2O_3 concentrations indicative of ARC and MORB tectonic
388 environments which is typical of the Guiana shield; consisting of volcanic arc segments accreted
389 over an Archean core (Tassinari 1997; Cordani & Teixeira 2007; Daoust et al. 2011; Reis et al.
390 2000; Fraga et al. 2009; Kroonenberg et al. 2016).

391 **Paleo-thermal conditions of the mantle**

392 The concentration and aggregation state of lattice bound nitrogen in diamond provides
393 additional constraints on the crystallization temperature and mantle residence conditions of
394 Guyanese diamonds. Nitrogen is the most abundant impurity in diamond, with concentrations
395 sometimes reaching >0.3 wt% (Woods et al. 1990; Cartigny et al. 2001; Stachel and Harris 2009;
396 Smart et al. 2011). Quantitative and FTIR derived nitrogen concentrations range from trace to
397 1971 ppm, with population means from different localities ranging between 120 and 620 ppm
398 (Fig. 5a). Guyanese diamonds are predominantly Type I, including Type IaAB, Type IaA, and
399 Type IaB. When compared to other South American diamonds (Kamarang, Kurupung,
400 Konawaruk and Maikwak), nitrogen concentrations are within similar ranges to diamonds from
401 Canastra and Arenópolis, Brazil (Table 6). The aggregation state of nitrogen within diamond is
402 largely a function of residence temperature (Chrenko et al. 1977; Evans and Qi 1982). Kinetic
403 modelling of the change in nitrogen aggregation state can be used to quantify the thermal
404 evolution of the continental lithosphere and paleotectonic processes (Taylor et al. 1990).
405 Individual total N ppm vs. $\%N_B$ (degree of nitrogen aggregation) ratios were used to calculate
406 mean residence temperatures of $1124 \pm 100^\circ\text{C}$ (Fig. 5) using the kinetics of the nitrogen A-B
407 center aggregation reaction (e.g., Taylor et al. 1990; Taylor et al. 1996). Residence temperature
408 distribution is slightly negatively skewed and slightly leptokurtic (Table 7). We considered a
409 minimum age of eruption of 2.0 Ga and an assumed residence time of 1.3 Ga, if Guyana's

410 diamonds are derived from the Roraima Supergroup (maximum age of peridotitic diamonds ~
411 3.3 Ga – maximum age of Roraima Supergroup ~ 2.0 Ga). We also considered the possibility
412 that Guyana’s diamonds might be derived from more recent kimberlites, of which the youngest
413 of the Guiana Shield have an eruption age of ~ 0.7 Ga (Channer et al. 2001) and an assumed
414 residence time of 2.6 Ga (maximum age of peridotitic diamonds 3.3 Ga – maximum age of
415 Guianamo kimberlites ~ 0.7 Ga). Assumptions regarding residence times ranging from the
416 Paleoproterozoic of 1.3 Ga and Neoproterozoic of 2.6 Ga vary residence temperature by less than
417 3%. These formation temperatures indicate that both diamond populations can be derived from
418 similar thermal conditions beneath the Guiana Shield, despite a wide range in possible
419 emplacement ages. Projecting the average residence temperature along geothermal gradients of
420 38 - 42 mW/m² gives minimum crystallization depths between 165 and 185 km, which is
421 evidence for crystallization in the lithospheric mantle (Stachel and Harris 2009).

422 **Magma composition**

423 Diamond habit, size, and form reflect crystal development during growth in the mantle,
424 whereas dissolution and abrasion textures reveal resorption during ascent and transport,
425 respectively. Guyana’s diamonds are predominantly octahedral (Fig. 3a), indicating slow growth
426 in near-equilibrium conditions found beneath a thick and stable subcratonic lithosphere in the
427 diamond stability field (Harrison and Tolansky 1964; Seal 1965; Sunagawa 1984; Stachel and
428 Harris 2009). Dodecahedrons (Fig. 3b) represent the second most common crystal habit for
429 diamonds across Guyana; this form is particularly observed at Ekereku. Dodecahedrons may
430 form in the mantle or during magmatic ascent via dissolution of octahedron apices and edges in
431 response to disequilibria produced by high temperature oxidation in the presence of CO₂ and
432 H₂O fluid phases (Fedortchouk et al. 2007). Diamond populations from other regions in Guyana

433 do not preserve a distribution so enriched in dodecahedral form, providing evidence for different
434 conditions of mantle departure or host magma volatile contents.

435 Additional aspects of the diamond-entraining magmatic fluid can be inferred from
436 dissolution features on crystal faces. Chemical oxidation caused by the interaction of fluid
437 volatile phases in a kimberlite or related rock, exploits surface defects on a diamond, causing it
438 to dissolve. Dissolution produces pits and hillocks, whose geometries are controlled by internal
439 dislocations, crystal defects, and intensive variables including pressure, temperature, and fO_2
440 (Fedortchouk 2015). Dissolution features (Fig. 3f) occur on 95% of the diamonds. Teardrop
441 hillocks are the most common resorption texture and indicate moderate resorption (Tappert and
442 Tappert 2011). Many different pit dissolution textures are recognized but are indistinguishable
443 amongst different geographic locations. Flat and point bottomed trigons, tetragons, and hexagon
444 pits are observed. Coarse flat bottom trigons are evidence for pre-eruptive mantle/melt
445 dissolution at temperatures ranging from 1250 to 1300°C (Fedortchouk 2015). Average diamond
446 residence temperatures of ~1120°C and mantle/melt dissolution temperatures of 1250 to 1300°C
447 suggest diamonds encounter variable mantle thermal conditions during residence, such as higher
448 temperatures of kimberlitic melt during ascent. The greater abundance of flat bottom trigons
449 relative to point bottom trigons in abraded diamond populations indicates that the erupting host
450 magma was enriched in H₂O relative to CO₂ (Fedortchouk 2015). Experimental data confirm that
451 dissolution pit textures begin as point bottom features. In a fluid enriched in H₂O relative to
452 CO₂, dissolution of the diamond proceeds more rapidly in the lateral direction rather than the
453 vertical or {111} direction, creating coarse and flat-bottomed pits (Fedortchouk 2015). Late
454 stage etching microdisk textures (Fig. 3g) found on ~5% of the diamonds also provide evidence
455 for an H₂O-rich magma. These features form when the surface of the diamond is etched by a

456 H₂O fluid phase in the ascending host magma (Fedortchouk et al. 2007). Kimberlite magmas are
457 inferred to be often CO₂-rich and have a high CO₂/H₂O ratio (Sparks 2013). The dissolution
458 textures observed in Guyana's diamonds instead suggest that both abraded and non-abraded
459 diamond populations were hosted by a magma with more H₂O, and therefore a lower CO₂/H₂O
460 ratio. This characteristic is more commonly inferred for lamproitic melts (Bergman 1987;
461 Mitchell and Bergman 1991) although H₂O-rich kimberlite melts are possible (e.g., Ekati mine
462 kimberlites, see Fedortchouk et al. 2010). Because the non-abraded diamonds present a greater
463 proportion of point bottom dissolution textures than abraded diamonds, these diamonds may
464 have been entrained in a different host melt with a different ratio of H₂O/CO₂.

465 **Abraded versus non-abraded diamonds**

466 Diamond is strongly resistant in the natural environment to abrasion. It is brittle, which
467 permits only microcleavage abrasion in the faceting process, and it is extremely hard (Wilks and
468 Wilks 1972; Oganov et al. 2013). Accordingly, percussive marks, scratches, and edge abrasion
469 textures require repeated cycles of erosion, transport and deposition and/or a lengthy residence
470 time within surface environments. Using abrasion textures, we recognized two populations of
471 alluvial diamonds. Pristine, non-abraded diamonds account for 15% of all diamonds. Ekereku
472 has the highest relative proportion of non-abraded diamonds. Jawalla, Konawaruk, Maikwak and
473 Monkey Mt. have no abraded diamonds, but we acknowledge that the sample sizes from those
474 regions are small.

475 The non-abraded stones are found in the same deposits as the abraded diamonds.
476 Nitrogen concentrations indicate that non-abraded and abraded groups may have statistically
477 distinct subpopulations, six of which are common to both groups. These shared subpopulations
478 suggest that some diamonds are sourced from similar mantle residence and thermal conditions.

479 The distinct subpopulations identified in only the abraded or non-abraded groups may reflect
480 isolated mantle and emplacement conditions. Statistically distinct spectroscopic responses
481 between abraded and non-abraded populations also present evidence for different provenance
482 and source (Table 4). Ultraviolet luminescence responses in abraded diamonds are
483 overwhelmingly green and non-responsive, whereas non-abraded diamonds are split between
484 non-responsive or green (Fig. 4). Luminescence is caused by the presence of impurities, such as
485 nitrogen, and related defects which create vacancy centers in diamonds. Combined substitutional
486 nitrogen and vacancy centers (H3 and H4 defects) within the diamond produced by irradiation
487 followed by high temperature annealing are commonly ascribed to green luminescence (Shigley
488 and Breeding 2013). This suggests that Guyana's abraded diamond population, which have a
489 greater proportion of luminescent green stones were subjected to some form of metamorphic
490 overprint. Abraded diamonds cathodoluminesce predominantly green, with moderate to minor
491 blue and other colors. The majority of non-abraded diamonds cathodoluminesce blue.
492 Worldwide, most diamonds from unmetamorphosed deposits cathodoluminesce blue with zero
493 phonon line emissions at 415-440 nm and 480-490nm (Bulanova et al. 1995; Lindblom et al.
494 2005). This is attributed to the N3 defect where three nitrogen atoms surround a vacancy. With
495 increasing grades of metamorphism and mild annealing at higher temperatures, nitrogen related
496 defect centers become increasingly more complex and blue CL shifts to other colors, with
497 emissions between 490-670 nm (Bruce et al. 2011; Kopylova et al. 2011). In diamond, vacancies
498 and interstitials become more mobile at 500-800°C and ~300°C respectively (Clark et al. 1992;
499 Collins et al. 2005; Collins and Kiflawi 2009). Enhanced diffusion and entrapment of vacancies
500 and interstitials at higher temperatures at the site of various nitrogen forms to produce new
501 optical centers is likely how blue CL shifts to other colors (Iakoubovskii and Adrianssens 1999;

502 Collins and Ly 2002). In the crust, these temperatures are typically inferred for zeolite to
503 greenschist facies metamorphic environments. The abraded population likely experienced some
504 metamorphic overprint. Comparatively, non-abraded diamonds may have been less
505 metamorphosed. This can be also influenced by pre-existing nitrogen and vacancy related defects
506 (N₃, NV^o, and NVN) in Type Ia diamonds and manifest as photoluminescence emissions more
507 commonly at 575 nm and less so at 430-450 nm but correlates rarely with cathodoluminescence
508 (Bruce et al. 2011). Alternatively, irradiation damage during long placer residence would create
509 charge vacancies and interstitials in the diamond lattice, which would also shift CL emittance
510 from blue to other colors, but this damage is usually more common within the first 25 microns of
511 the diamond surface (Vance et al. 1973; Breeding et al. 2018). Abraded diamonds are also larger
512 in mass (9.3 ± 2.2 mg) than non-abraded diamonds (5.5 ± 4.2 mg), present fewer dodecahedral
513 forms, and a greater ratio of flat-bottom to point-bottom dissolution textures (5:1 compared to
514 1:1). This is evidence that abraded and non-abraded diamond populations may have been
515 entrained in different host melts. At present, both abraded and non-abraded populations are
516 mixed into the same alluvial deposits, reflecting a complex interplay of mantle storage, eruptive
517 history, and fluvial transport throughout the > 2.5 Ga evolution of the Guiana Shield.

518 **Provenance**

519 Abrasion, nitrogen concentration, CL, and UV observations indicate that alluvial deposits
520 from each productive region across Guyana host both abraded, metamorphosed, nitrogen-poor
521 diamonds as well as non-abraded, less metamorphosed, nitrogen-rich diamonds. Guyana's
522 abraded diamonds are most likely derived from recycled paleo-placers with a metamorphic
523 overprint. The probable source is the greenschist facies pebbly conglomerates or volcanoclastics
524 of the 1.98 to 1.78 Ga Roraima Supergroup. Diamondiferous alluvial deposits occur in close

525 proximity to the margin of the Roraima Supergroup. In addition, diamond-bearing alluvial
526 deposits contain abundant quartzite and jasper clasts derived from the nearby Roraima
527 Supergroup. The Roraima Supergroup has been exposed at the surface since at least the early
528 Mesozoic (McConnell 1968). Increased weathering and erosion associated with rifting and
529 opening of the Atlantic since the Jurassic produced initial alluvial deposits derived from the
530 Roraima Supergroup, which have been continually exhumed and redeposited since that time by
531 repeated cycles of river capture, rejuvenation, degradation and aggradation (McConnell 1968,
532 Gibbs and Barron 1993). The majority of diamond populations in Guyana were likely abraded
533 within this complex polycyclic alluvial environment. Non-abraded diamonds were also likely
534 sourced from the Roraima Supergroup basal conglomerates and volcanoclastic horizons but were
535 trapped in sediment packages that experienced less energetic deposition, reworking and
536 experienced less metamorphic overprint and longer primary storage.

537 The Roraima Supergroup source is supported by comparison to alluvial diamond deposits
538 in Mutum, Brazil. Mutum diamonds are mined from alluvial terraces shed from conglomerates of
539 the Tepequém Formation in Brazil (Santos et al. 2003; Reis et al. 2017). The diamonds are
540 similar to Guyana's diamonds in size, skin color, $\delta^{13}\text{C}$, and nitrogen concentrations. These
541 diamonds, however, also present more flattened forms (60%), grey diamonds (40%), and fewer
542 proportions of diamonds with trigons (Araújo et al. 2011). This suggests that these diamonds
543 may be derived from a different magma source than Guyana's diamonds. The Arai Formation of
544 the Roraima Supergroup is the local age and lithologic equivalent of the Tepequém Formation.
545 Accordingly, conglomerates and volcanoclastics of the Arai Formation may be the detrital source
546 of Guyana's diamonds, representing a regional Paleoproterozoic high energy, siliciclastic

547 depositional basin that was a sink for diamonds emplaced by several episodes of kimberlite
548 volcanism within the Guiana Shield, during the middle Paleoproterozoic or older (>2.0 Ga).

549 Other hypotheses regarding the source of the diamonds have been put forward over the
550 past decades, including sources in West Africa, Boa Vista (Brazil), Dachine (French Guiana),
551 and Guaniumo (Venezuela). West Africa is home to kimberlite and alluvial diamond deposits.
552 Most diamonds from West Africa are alluvial in origin, but diamonds have also been mined from
553 kimberlites (Deines and Harris 1995; Skinner et al 2004). The alluvial diamonds are largely
554 weathered from Mesozoic kimberlite pipes and dykes. Colorless to brown body color and green
555 skins are common; similar to those in Guyana (Sutherland 1982; Janse 1996; Stachel et al. 2002).
556 Size and quality are inversely related to distance from the kimberlite source (Knopf 1970;
557 Norman et al. 1996; Grantham and Allen 1960; Janse 1996). The smallest carat sizes and best
558 quality gems are found in beach placers along the West African coastline. The oldest Mesozoic
559 sources may have produced microdiamonds that could have reached Guyana's eastern coast prior
560 to rifting associated with the Atlantic Ocean, but diamonds are not found on the coast. The more
561 recent Mesozoic kimberlites are too young and shed detrital diamonds into the juvenile Atlantic
562 Ocean instead. We conclude that Guyana's diamonds are unlikely to be related to sources in
563 West Africa.

564 The closest primary diamond-bearing igneous sources in the modern tectonic setting are
565 the Guaniumo kimberlite dykes in Venezuela and metamorphosed ultramafic and pyroclastic
566 shoshonites or lamprophyres in Dachine, French Guiana (Capdevila et al. 1999; Channer et al.
567 2001; Kaminsky et al. 2000; Kaminsky et al. 2004; Smith et al. 2016). Although some
568 similarities exist, including upper mantle temperatures, sizes, and colors between Guyana's and
569 Guaniumo's diamonds, we contend that those sources are unlikely to be genetically associated

570 with Guyanese diamonds based on geographic distance, distinct ^{13}C signatures, nitrogen
571 aggregation, predominantly eclogitic inclusions, and CL responses (Channer et al. 2001;
572 Kaminsky et al. 2000; Kaminsky et al. 2004). Furthermore, Dachine diamonds are smaller (< 1
573 mm), have a lower total nitrogen range from trace to 110 ppm, are strictly Ib to IaA, and have
574 mostly sulfide inclusions (Smith et al. 2016).

575 Detrital zircon geochronology provides additional compelling evidence supporting
576 provenance. Detrital zircon U-Pb ages from both colluvial and alluvial sediment demonstrate that
577 these diamondiferous deposits are likely derived from rocks of late Trans-Amazonian age, with
578 lesser contributions of Archean grains (Fig. 8). These deposits are inferred to be Pleistocene to
579 recent in age (McConnell 1968; Gibbs and Barron 1993). The similar ages between the diamond-
580 bearing colluvium and alluvium is consistent with the interpretation that both types of placer
581 diamond deposit are derived from similarly aged bedrock sources of the Barama-Mazaruni group
582 such as Surumu group volcanoclastics (Basei 1978; Schobbenhaus et al. 1994; Reis et al. 2017),
583 or alternatively, as inherited minerals from the once extensive Roraima Supergroup in a foreland
584 basin fill (Santos et al. 2003). The dominantly unimodal characteristic of these detrital zircon age
585 spectra is consistent with derivation from a relatively small geographic region, as a more multi-
586 modal age distribution would be expected if the diamond-bearing sediment was sourced from a
587 large fluvial catchment. Furthermore, the narrow range of ages suggesting a local geographic
588 origin, preponderance of coarse quartz and jasper lithic fragments, and presence of non-
589 kimberlitic or related rock type indicator minerals, lends evidence to the Roraima Supergroup
590 being the provenance area for the Guyana detrital zircons and diamonds.

591 **Implications**

592 In an environment prone to extreme tropical weathering, Guyana's diamonds are likely
593 the only remaining mantle xenocrysts which can offer insight into volcanic and tectonic controls
594 that existed during the early evolution of the Guiana Shield. Detrital zircon U-Pb ages suggest
595 that the kimberlite or related rock sources that erupted Guyana's diamonds represent episodes of
596 kimberlite volcanism during at least the middle Paleoproterozoic or during the Archean. Also,
597 the surfaces of diamonds demonstrate they were emplaced by various mantle-derived melts
598 enriched or balanced in H₂O relative to CO₂. Guyana's diamonds are likely xenocrysts from
599 some of the Earth's oldest kimberlites or lamproites. These source rocks have long since eroded
600 or are still undiscovered.

601 Guyana's diamonds are divided into two populations of recycled and abraded diamonds
602 and primary and non-abraded diamonds. Both abraded and non-abraded diamonds, can be
603 distinguished according to unique spectroscopic, luminescence and morphological
604 characteristics. This classification can aid in characterizing the prospectivity of underexplored
605 diamond fields, especially when other mantle xenocrysts are absent. The abraded diamonds are
606 likely recycled detrital grains eroding from rocks of the Roraima Supergroup, which could
607 therefore represent a regional placer diamond source terrane with a lateral extent of at least
608 450,000 km². The provenance of non-abraded diamonds still remains enigmatic. It may be that
609 there are undiscovered primary kimberlites but it is more likely that these non-abraded diamonds
610 may also be sourced from the Roraima Supergroup basal conglomerates and volcaniclastic
611 horizons which have experienced less metamorphic overprint. Both diamond populations,
612 inclusion suites, $\delta^{13}\text{C}$, and nitrogen concentrations suggest diamond formation at residence
613 temperatures of approximately 1120°C in the peridotitic and eclogitic lithospheric mantle of the
614 Guiana Shield.

615
616
617
618
619
620
621
622
623
624
625
626
627
628
629
630
631
632
633
634
635

Acknowledgements

We thank Marcus Harden of Alicanto Minerals and Gordon Nestor of the Guyana Geology and Mines Commission for their logistical support. Avalon Jagnandan of the Guyana Gold and Diamond Miners Association. Roy Melville and Nigel Blackman provided invaluable on field support, for which we are grateful. We also thank James Krakowsky (General Manager for Kays Diamond Enterprise Ltd), for technical advice and diamond samples, which were crucial to this study. A special thanks is given to Maya Kopylova of the University of British Columbia for her technical input. We thank Barry Schaulis at the University of Arkansas for assistance with LA-ICP-MS data collection.

References

Andrews-Jones, D.A. 1968. Petrogenesis and geochemistry of the rocks of the Kenema district, Sierra Leone (PhD thesis abs.). Leeds University, England.

Araújo, D.P., Santos, R.V., Souza, V., Chemale F. e Dantas, E. (2011) Diamantes Serra do Tepequém: resultados preliminares. 12th Simpósio da Amazônia, 2 a 5 de outubro de 2011 - Boa Vista - Roraima. Documento da Conferência.

Basei, M.A.S., and Teixeira, W. (1975) Geocronologia do Território de Roraima, in Anais, Conferência Geológica Intergüianas, 10th, Belém, Brazil: Belém, Brazil, Departamento Nacional de Pesquisa Mineral, 453–473.

Bassoo, R. and Murphy, B. (2018) The 9 Mile deposit of the Barama-Mazaruni Greenstone belt of the Guiana Shield: Geochemistry, geochronology and regional significance. Brazilian Journal of Geology, 48, 671-683.

- 636 Bardet, M.G., and Vachette, M. 1966. Determination d'ages de kimberlites de l'ouest African et
637 assai d'interpretation de dataions des diverses venus diamantiferes dans le monde. Bur.
638 Rech. Geol. Min. Rep. D866A59.
- 639 Bergman, S.C. (1987) Lamproites and other potassium-rich igneous rocks, a review of their
640 occurrence, mineralogy and geochemistry. Geological Society of London, Special
641 Publications, 30, 103 -190.
- 642 Bosma, W., Kroonenberg, S.B., van Lissa, R. V., Maas, K., and de Roever, E.W.F. (1983)
643 Igneous and metamorphic complexes of the Guiana Shield in Suriname. Geol. Mijnbouw,
644 62, 241-254.
- 645 Briceno, H.O. (1984) Genesis of Venezuelan mineral deposits II. Acta Scientifica Venezuelana
646 36.
- 647 Breeding, C.M., Eaton-Magaña, S., and Shigley, J.E. 2018. Natural-color green diamonds: A
648 beautiful conundrum. Gems and Gemology. 54: 2-27.
- 649 Bruce, L. F., Kopylova, M.G., Longo, M., Ryder, J., and Dobrzhinetskaya, L.F. (2011)
650 Luminescence of diamonds from metamorphic rocks. American mineralogist, 96, 14-22.
- 651 Bulanova, G.P. (1995) The formation of diamond. Journal of Geochemical Exploration,
652 53, 1-23.
- 653 Cabral, N.I., Nannini, F., Silveira, F.V., Cunha, L.M., Bezerra, A.K., Souza, W.S. (2017) Mapa
654 das áreas kimberlíticas e diamantíferas dos estados de Roraima, Pará, Piauí, Rio Grande
655 do Norte, Santa Catarina e Rio Grande do Sul. Programa Geologia do Brasil (PGB), Ação
656 Avaliação dos Recursos Minerais do Brasil. Natal, CPRM, 2017, 1 mapa colorido, 215 x
657 90 cm. Escala 1:5,000,000.
- 658 Capdevila, R., Arndt, N., Letendre, J., Sauvage, J.F. (1999). Diamonds in volcanoclastic

- 659 komatiite from French Guiana. *Nature*, 399, 456–458.
- 660 Cartigny, P. (2005) Stable isotopes and the origin of diamond. *Elements*, 1, 79-84.
- 661 Cartigny, P., De Corte, K., Vladislav, S., Ader, M., De Parpe, P., Sobolev, N.K. and Javoy, M.
662 (2001) The origin and formation of metamorphic microdiamonds from the Kokchetav
663 massif, Kazakhstan: a nitrogen and carbon isotopic study. *Chemical Geology*, 176, 265-
664 281.
- 665 Cartigny, P., Palot, M., Thomassot, E., and Harris, J.W. (2014) Diamond formation: a stable
666 isotope perspective. *Annual review of Earth and Planetary Sciences*, 42, 699-732.
- 667 Channer, D.M.DER., Egorov, A. and Kaminsky, F. (2001) Geology and structure of the
668 Guaniamo diamondiferous kimberlite sheets, south-west Venezuela. *Revista Brasileira de*
669 *Geociências*, 31, 615-630.
- 670 Chrenko, R.M, Tuft, R.E., and Strong, H.M. (1977) Transformation of the state of nitrogen in
671 diamond. *Nature*, 20, 141-144.
- 672 Clark, C.D., Collins, A.T., and Woods, G.S. (1992) Absorption and luminescence spectroscopy.
673 In J.E. Field, Ed., *The Properties of Natural and Synthetic Diamond*, 35–69. Academic,
674 New York.
- 675 Collins, A., Connor, A., Ly, C-H., and Shareef, A. (2005) High-temperature annealing of optical
676 centers in type-I diamond. *Journal of Applied Physics*, 97, 083517.
- 677 Collins, A. and Kiflawi, I. (2009) The annealing of radiation damage in Type Ia diamond.
678 *Journal of Physics: Condensed Matter*, 21, 364209.
- 679 Collins, A. and Ly, C-H. (2002) Misidentification of nitrogen-vacancy absorption in diamond.
680 *Journal of Physics: Condensed Matter*, 14, L467–L471.

- 681 Cordani U.G. and Brito Neves B.B. (1982) The geologic evolution of South America during the
682 Archaean and early Proterozoic. *Revista Brasileira de Geociências*, 12,78-88.
- 683 Cordani U.G., Teixeira W. (2007) Proterozoic accretionary belts in the Amazonian Craton.
684 *Geological Society of America Memoirs*, 200, 297-320.
- 685 Da Silva Rodrigues, A.F. (1991) Depositos diamantíferos de Roraima, in Schobbenhaus, C.,
686 Queiroz, E.T., and Coelho, C.E.S., eds., *Principais depósitos minerais do Brasil. Rochas e*
687 *minerais industriais. Gemas e rochas ornamentais: Brasília, Departamento Nacional de*
688 *Produção Mineral (DNPM)/Companhia de Pesquisa de Recursos Minerais (CPRM)*, 177-
689 198.
- 690 Daoust C., Voicu G., Brisson H. and Gauthier M. (2011) Geological Setting of the
691 Paleoproterozoic Rosebel gold district, Guiana Shield, Suriname. *Journal of South*
692 *American Earth Sciences*, 32, 222-245.
- 693 Deines, P., and Harris, J.W. (2004) New insights into the occurrence of ^{13}C -depleted carbon in
694 the mantle from two closely associated kimberlites: Letlhakane and Orapa, Botswana.
695 *Lithos*, 77, 125-142.
- 696 Deines, P., and Harris, J.W. (1995) Sulfide inclusion chemistry and carbon isotopes of African
697 diamonds. *Geochemica Cosmochemica Acta*, 59, 3173-3188.
- 698 Delor C., Lahondère D., Egal E., Lafon J.M., Cocherie A., Guerrot C., Rossi P., Truffert C.,
699 Théveniaut H., Phillips D. and de Avelar V.G. (2003) Trans-Amazonian crustal growth
700 and reworking as revealed by the 1:500,000 scale geological map of French Guyana (2nd
701 edition). *Geology of France and surrounding areas. Special Guyana Shield, BRGM –*
702 *SGF*, 2-3-4:5–57.

- 703 Evans, T. and Qi, Z. (1982) The kinetics of the aggregation of nitrogen atoms in diamond.
704 Proceedings of the Royal Society A, 381, 169-178.
- 705 Fedortchouk, Y., Canil, D., and Semenets, E. (2007) Mechanisms of diamond oxidation and their
706 bearing on the fluid composition in kimberlite magmas. American mineralogist, 92,
707 1200-1212.
- 708 Fedortchouk, Y. (2015) Diamond resorption features as a new method for examining conditions
709 of kimberlite emplacement. Contributions to mineralogy and petrology. 170.
- 710 Fedortchouk, Y., Matveev, S., Carlson, J.A. (2010) H₂O and CO₂ in kimberlitic fluid as recorded
711 by diamonds and olivines in several Ekati Diamond Mine kimberlites, Northwest
712 Territories, Canada. Earth and Planetary Science Letters, 289, 549-559.
- 713 Fourie, L., Phillips, D., Kieviets, G., 1998. Ages of Koidu kimberlites, Sierra Leone,
714 Unpublished De Beers data.
- 715 Fourie, L., Barton, E., Kieviets, G., 2000. Ages of Guinea kimberlites, Sierra Leone,
716 Unpublished De Beers data.
- 717 Fraga, L.M.B., Macambira, M.J.B., Dall'Agnol and R., Costa, J.B.S. (2009) 1.94–1.93 Ga
718 charnockitic magmatism from the central part of the Guyana Shield, Roraima, Brazil:
719 single-zircon evaporation data and tectonic implications. Journal of South American
720 Earth Sciences, 27, 247-257.
- 721 Galbraith, R., and Green, P. (1990) Estimating the component ages in a finite mixture.
722 International Journal of Radiation Applications and Instrumentation. Part D. Nuclear
723 Tracks and Radiation Measurements, 17, 197-206.
- 724 Gibbs A.K. and Barron C.N. (1993) The Geology of the Guiana Shield. Oxford University Press,
725 New York.

- 726 Grantham, D.R., and Allen, J.B. (1960) Kimberlite in Sierra Leone. Overseas Geology and
727 Mineral Resources, 8(1), 5-25.
- 728 Hall, P.K. 1972. The diamond fields of Sierra Leone. Geological Survey of Sierra Leone
729 Bulliten. 5(1): 133
- 730 Harrison, E.R., and Tolansky, S. (1964) Growth history of a natural octahedral diamond.
731 Proceedings of the Royal Society of London. Series A, mathematical and physical
732 sciences, 279, 490-496.
- 733 Heesterman, L., Kemp A.W., Arjune B.K., and Cole, E. (2005) Pashanamu project geology,
734 structure and geochemistry. Guyana Geology and Mines Commission.
- 735 Howell, D., O'Neill, C. J., Grant, K. J., Griffin, W. L., Pearson, N. J., and O'Reilly, S. Y. (2012)
736 μ -FTIR mapping: distribution of impurities in different types of diamond growth.
737 Diamond and Related Materials, 29, 29-36.
- 738 Iakoubovskii, K. and Adriaenssens, G.J. (1999) Photoluminescence in CVD diamond films.
739 Physica Status Solidi Applied Research, 172, 123–129.
- 740 Janse, A.J.A. (1996) A history of diamond sources in Africa: Part II. Gems and Gemology.
- 741 Kaminsky, F.V., and Khachatryan, G. (2012) Nitrogen in diamond. KM Diamond Exploration,
742 Ltd. West Vancouver, Canada. Indian Institute of Technology, Mumbai.
- 743 Kaminsky F.V., Zakharchenko O.D., Khachatryan G.K., and Shiryaev A.A. (2001) Diamonds
744 from the Coromandel area, Minas Gerais, Brazil. Revista Brasileira de Geociências, 31,
745 583-596.
- 746 Kaminsky, F.V., Sablukov, S.M., Sablukova, L.I. and Channer, D.M.DER. (2004)
747 Neoproterozoic “anomalous” kimberlites of Guaniamo, Venezuela: mica kimberlites of
748 “isotopic transitional” type. Lithos, 76, 565-590.

- 749 Kaminsky, F.V., Zakharchenko O.D., Khachatryan G.K., Griffin W.L., and Channer D.M.DeR.
750 (2006). Diamond from the Los Coquitos area, Bolivar State Venezuela. The Canadian
751 Mineralogist, 44, 323-340.
- 752 Kaminsky, F.V., Zakharchenko, O.D., Griffin, W.L., Channer, D.M.DER. and Khacchatryan-
753 Blinova, G.K. (2000). Diamond from the Guaniamo area, Venezuela. Can. Mineral, 38,
754 1347-1370.
- 755 Kiviets, G.B. 2003. $^{40}\text{Ar}/^{39}\text{Ar}$ laser probe analysis of phlogopite from two samples from the
756 Weasua area, Western Liberia. Unpublished De Beers data.
- 757 Knopf, D. (1970) Les kimberlites et les roches apparentées de Côte d'Ivoire (Kimberlite and
758 related rocks of Ivory Coast). Sodemi, Abidjan. pp 202.
- 759 Kopylova, M., Afanasiev, V.P., Bruce, L.F., Thurston, P.C., and Ryder, J. (2011)
760 Metaconglomerate preserves evidence for kimberlite, diamondiferous root and medium
761 grade terrane of a pre-2.7 Ga Souther Superior protocraton. Earth and Planetary science
762 letters, 312, 231-225.
- 763 van Kooten, C. (1954) Eerste onderzoek op diamant: Rosebel-Sabanpassie. Mededeling
764 Geologisch Mijnbouwkundige Dienst, Suriname 11, 63-64 pp.
- 765 Kroonenberg S.B., De Roever E.W.F., Fraga L.M., Reis N.J., Faraco M.T., Cordani U.G., Lafon
766 J.M. and Wong, Th. E. (2016) Paleoproterozoic evolution of the Guiana Shield in
767 Suriname - a revised model . Netherlands Journal of Geosciences, 95, 491-522.
- 768 Kroonenberg, S.B., and Gersie, K. (2019) Quaternary climate change and its importance for gold
769 exploration in the Guiana Shield. Conference paper. 11th Inter Guiana Geological
770 Conference, Paramaribo, Suriname, 19-20 February, 2019.

- 771 Lafuente, B., Downs, R. T., Yang, H., and Stone, N. (2016) The power of databases: the RRUFF
772 project. In Highlights in mineralogical crystallography (pp. 1-29). Walter de Gruyter
773 GmbH.
- 774 Liang, P., and Forman, S. (2019) LDAC: Luminescence dose and age calculator (v 1.0)
775 [computer software]. Luminescence dating research lab. Baylor University.
- 776 Lindblom, J., Holsa, J., Papunen, H., and Hakkanen, H. (2005) Luminescence study of defects in
777 synthetic as-grown and HPHT diamonds compared to natural diamonds. American
778 Mineralogist, 90, 428–440.
- 779 Mather, K.A., Pearson, D.G., McKenzie, D., Kjarsgaard, B.A., and Priestly, K. (2011)
780 Constraints on the depth and thermal history of the cratonic lithosphere from peridotite
781 xenoliths, xenocrysts and seismology. Lithos, 125, 729-742.
- 782 Magee, C.W. and Taylor, W.R. 1999. Diamond and chromite geochemical constraints on the
783 nature of the Dachine complex, French Guiana, Annual Report. Australian National
784 University, Canberra, Australia: 85.
- 785 McConnell, R.B. (1968) Planation surfaces in Guyana. The Geographical Journal, 134, 506-520.
- 786 McLachlan, G. J., Lee, S. X., and Rathnayake, S. I. (2019) Finite Mixture Models: Annual
787 Review of Statistics and Its Application, 6(1), 355-378.
- 788 Meyer, H.O.A, and McCallum, M.E. (1993) Diamonds and their sources in the Venezuelan
789 portion of the Guyana Shield. Economic Geology, 88, 989-998.
- 790 Mitchell, R.H. and Bergman, S.C. (1991) Petrology of lamproites. Plenum Press. New York and
791 London.

- 792 Nadeau, S., and Heesterman, L. (2010) Guyana Geology and Mines Commission, Geological
793 Map of Guyana - scale 1: 1 million. Guyana Geology and Mines Commission,
794 Georgetown, Guyana.
- 795 Naipal, R., Kroonenberg, S., and Mason, P. (2019) Ultramafic rocks of the Paleoproterozoic
796 greenstone belt in the Guiana Shield of Suriname, and their mineral potential. SAXI- XI
797 Inter Guiana Geological Conference 2019: Paramaribo, Suriname.
- 798 Norcross C.E. (1997) U-Pb Geochronology of the Omai Intrusion Hosted Au- Quartz Vein
799 Deposit and Host Rocks, Guiana Shield, South America. A Thesis submitted in
800 conformity with the requirements for the degree of Master of Science, Graduate
801 Department of Geology, University of Toronto. University of Toronto.
- 802 Norman, D.I., Ward, J., McKittrick, S. (1996) Hosts and sources of Ghana diamonds. Paper
803 given at the SME/AIME annual meeting, Phoenix, Arizona, USA.
- 804 Oganov, A., Hemley, R.J., Hazen, R.M. and Jones, A.P. (2013) Structure, Bonding, and
805 Mineralogy of Carbon at Extreme Conditions. *Reviews in Mineralogy and Geochemistry*,
806 75. 47-77.
- 807 Olszewski, W.J., Jr., and Gaudette, H., and Mendonza, V. 1977. Rb-Sr geochronology of the
808 basement rocks, Amazonas Territory, Venezuela: a progress report. *Proc. V Congreso*
809 *Geologico Venezolano*, 2: 519-525.
- 810 Paton, C., Hellstrom, J., Paul, B., Woodhead, J., & Hergt, J. (2011). Iolite: Freeware for the
811 visualisation and processing of mass spectrometric data. *Journal of Analytical Atomic*
812 *Spectrometry*, 26(12), 2508.
- 813 Persaud, K. (2010) The diamond industry and exploration for diamonds in Guyana, Guyana
814 Geology and Miners Commission.

- 815 Pollack, H.N. and Chapman, D.S. (1977) On the regional variation of heat flow, geotherms and
816 lithospheric thickness. *Tectonophysics*, 38, 179-196.
- 817 Priem H.N.A., Boelrijk N.A.I.M, Hebed E.H., Verdurmen E.A., Verschure R.H. (1973) Age of
818 the Precambrian Roraima Formation in Northeastern South America: Evidence from
819 Isotopic Dating of Roraima Pyroclastic Volcanic Rocks in Suriname. 84, 1677-1684.
- 820 Ramlal, S. (2018) An investigation of the Brincks intrusion and its relationship to the
821 surrounding gold deposits, Brokopondo, Suriname, South America. MSc thesis. Anton de
822 Kom University of Suriname, 146-147.
- 823 Reid, A.R. (1974) Proposed origin for Guianian diamonds. *Geology*, 2, 67-68.
- 824 Reis N.J., de Faria M.S.G., Fraga L.M. and Haddad R.C. (2000) Orosirian calc-alkaline
825 volcanism and the Orocaima event in the northern Amazonian Craton, eastern Roraima
826 State. *Revista Brasileira de Geociências*, 30, 380-383.
- 827 Reis, N.J., Nadeau, S., Fraga, L.M., Betiollo, L.M., Faraco, M.T.L., Reece, J. Lachhman, D. and
828 Ault, R. (2017) Stratigraphy of the Roraima Supergroup along the Brazil-Guyana border
829 in the Guiana Shield, Northern Amazonian Craton – results of the Brazil-Guyana
830 Geology and Geodiversity mapping project. *Brazillian Journal of Geology*, 47, 43-57.
- 831 Santos, J.O.S., Potter, P.E., Reis, N.J., Hartman, L.A., Fletcher, I.R., McNaughton, N.J. (2003)
832 Age, source and regional stratigraphy of the Roraima Supergroup and Roraima-like
833 outliers in northern South America based on U–Pb geochronology. *Geological Society of
834 America Bulletin*, 115, 331–348.
- 835 Schobbenhaus, C., Hoppe, A., Lork, A., and Baumann, A. (1994) Idade U/Pb do magmatismo
836 Uatumã no norte do cráton Amazônico, Escudo das Guianas (Brasil): Primeiros

- 837 resultados, in Anais, Congresso Brasileiro de Geologia, 37th, Camboriú, Brazil: Porto
838 Alegre, Brazil, Sociedade Brasileira de Geologia, 2, 395–397.
- 839 Schönberger, J.M.H., (1975) Diamond exploration between the Suriname and Saramacca Rivers
840 (NE Suriname) . Mededeling Geologisch Mijnbouwkundige Dienst 23, 228-238.
- 841 Schönberger, H, and de Roever, E.W.F. (1974) Possible origin of diamonds in the Guiana Shield:
842 Comment. Geology, 2, 475-475.
- 843 Schulze, D.J. (2003) A classification scheme for mantle-derived garnets in kimberlite: a tool for
844 investigating the mantle and exploring for diamonds. Lithos, 71, 195-213.
- 845 Schulze, D. J., Canil, D. M., Channer, D. M. DeR., Kaminsky, F.V. (2006) Layered mantle
846 structure beneath the western Guyana Shield, Venezuela: Evidence from diamonds and
847 xenocrysts in Guaniamo kimberlites. Geochimica et cosmochimica Acta, 70, 192-205.
- 848 Schwartz, G. (1978). Estimating the dimensions of a model. Annals of Statistics 6, 461-464.
- 849 Seal, M. (1965) Structure in diamonds as revealed by etching. American Mineralogist, 50, 105-
850 123.
- 851 Sharman, G. R., Sharman, J. P., & Sylvester, Z. (2018). DetritalPy: A Python-based toolset for
852 visualizing and analysing detrital geo-thermochronologic data. The Depositional Record,
853 4(2), 202-215.
- 854 Shields, H.N and Letendre, J. (1999) Final Exploration Report on Amatuk Prospecting License
855 for the period January 2, 1996 to February 9, 1998. Golden Star Resources Ltd.
- 856 Shigley, J.E., and Breeding, M. (2013) Optical defects in diamond: a quick reference chart.
857 Gems and Gemology, 49.
- 858 Skinner, E.M.W., Apter, D.B., Morelli, C., and Smithson, N.K. 2004. Kimberlites of the Man
859 Craton, West Africa. Lithos. 76: 233-259.

- 860 Slama, J., Košler, J., Condon, D.J., Crowley, J.L., Gerdes, A.E., Hanchar, J.M., Horstwood,
861 M.S., Morris, G.A., Nasdala, L., Norberg, N.S., Schaltegger, U., Schoene, B., Tubrett,
862 M., & Whitehouse, M.J. (2008). Plešovice zircon: a new natural reference material for
863 U-Pb and Hf isotopic microanalysis.
- 864 Smart, K., Chacko, T., Stachel, T., Muehlenbachs, K., Stern, R., and Heaman, L. (2011)
865 Diamond growth from oxidized carbon sources beneath the Northern Slave Craton,
866 Canada: a $\delta^{13}\text{C}$ -N study of eclogite-hosted diamonds from the Jericho kimberlite.
867 *Geochimica et Cosmochimica Acta*, 75, 6027-6047.
- 868 Smith, B.M., Walter J.W., Galina P.B., Mikhail S., Burnham A.D., Gobbo L., and Kohn S.C.
869 (2016) Diamonds from Dachine, French Guiana: A unique record of early Proterozoic
870 subduction. *Lithos*, 265, 82-95.
- 871 Stachel, T and Harris, J.W. (2009) Formation of diamond in the Earth's mantle. *Journal of*
872 *Physics: Condensed Matter*, 21, 364206 (10pp)
- 873 Stachel, T., Harris, J.W., Aulbach, S., and Deines, P. (2002) Kankan diamonds (Guinea) III: $\delta^{13}\text{C}$
874 and N characteristics of deep diamonds. *Contributions to mineralogy and petrology*, 142,
875 465 – 475.
- 876 Sunagawa, I. (1984) Morphology of natural and synthetic diamond crystals. In: I. Sunagawa
877 (editor) *Materials science of the Earth's interior*. Terra Scientific, Tokyo, 303-330.
- 878 Sutherland, D.G. (1982) The transport and sorting of diamonds by fluvial and marine processes.
879 *Econ. Geol.*, 77, 1613-1620.
- 880 Svisero, D.P., Shigley, J.E., and Weldon, R. (2017) Brazilian diamonds: A historical and recent
881 perspective. *Gems and Gemology*. 53(1).

- 882 Tappert, R. and Tappert, M. (2011) *Diamonds in nature: A guide to rough diamonds*. Springer
883 Heidelberg Dordrecht London New York.
- 884 Tappert, R., Stachel, T., Harris, J.W., Muehlenbachs, K. and Brey, G.P. (2006) Placer diamonds
885 from Brazil: Indicators of the composition of the Earth's mantle and the distance to their
886 kimberlitic sources. *Economic Geology*, 101, 453-470.
- 887 Tassinari C.C.G. (1997) The Amazonian Craton. In: De Wit M.J. and Ashwal M.J. (Editors),
888 *Greenstone Belts*. Clarendon Press, Oxford 558-566.
- 889 Taylor, W.R., Canil, D., Milledge, H.J. (1996) Kinetics of Ib to IaA nitrogen aggregation in
890 diamond. *Geochimica et Cosmochimica Acta*, 60, 4725-4733.
- 891 Taylor, W.R., Jaques, A.L. and Ridd, M. (1990) Nitrogen-defect aggregation characteristics of
892 some Australasian diamonds: Time-temperature constrains on the source regions of pipe
893 and alluvial diamonds. *American Mineralogist*, 75, 1290-1310.
- 894 Vance, E.R., Harris, J.W., and Milledge, H.J. (1973) Possible origins of α damage in diamonds
895 from kimberlite and alluvial sources. *Mineralogical magazine*. 39, 349-360.
- 896 Vanderhaeghe O., Ledru P., Thiéblemont D., Egal E., Cocherie A., Tegye M. and Milési J.P.
897 (1998) Contrasting mechanism of crustal growth Geodynamic evolution of the
898 Paleoproterozoic granite greenstone belts of French Guiana. *Precambrian Research*,
899 92, 165-193.
- 900 Westerman, A.R. 1969. A structural analysis of Mathews' ridge Mn mine – with an appendix on
901 supergene enrichment. Conference paper: Guiana geological conference. 8.
- 902 Wilks, E.M. and Wilks, J. 1972. The resistance of diamond to abrasion. *Journal of physics D:*
903 *Applied physics*. 5: 1902-1919.

- 904 Woods, G.S., Van Wyk, J.A. and Collins, A.T. (1990) The nitrogen content of type Ib synthetic
905 diamond. *Philosophical Magazine B*, 62, 589-595.
- 906 Wyman, D.A., O'Neill, C., Ayer, J.A. 2008. Evidence for modern-style subduction to 3.1 Ga; a
907 plateau-adakite-gold (diamond) association. In; Condie, K.C., Pease, V. (Eds.), *When did*
908 *plate tectonics begin on planet earth*: 129-148.
- 909 Xie, X., Mann, P., & Escalona, A. (2010). Regional provenance study of Eocene clastic
910 sedimentary rocks within the South America–Caribbean plate boundary zone using
911 detrital zircon geochronology. *Earth and Planetary Science Letters*, 291(1-4), 159-171.

912 **Figure captions**

- 913 Figure 1. Geological Map of the Guiana Shield and inferred adjacent West African craton during
914 the Jurassic, showing primary and placer diamond deposits. (AM – Amatuk, AR –
915 Arenópolis, BA – Baoule, BV – Boa Vista, CA – Canastra, CO – Los Coquitos, CR –
916 Coromandel, DC – Dachine, EK – Ekereku, GU – Guaniamo, JW – Jawalla, KM –
917 Kamarang, KU – Kurupung, KW – Konawaruk, MG – Mano Gadua, MK –
918 Maikwak, MM – Monkey Mt., NA – Nassau, RO – Rosebel, SE – Seguela, TE –
919 Tepequém, TO – Tongo, TY – Tortiya) (Modified from Santos et al. 2003, Nadeau
920 and Heesterman 2010, Daoust et al. 2011, Kroonenberg et al. 2016, and Bassoo and
921 Murphy 2018).
- 922 Figure 2. Body and skin color. a) colorless, b) white, c) yellow, d) brown, e) brown skins f)
923 green skins
- 924 Figure 3. Morphological features. a) octahedral, b) dodecahedral, c) flattened/macle, d) trigons,
925 e) hexagons, f) hillocks, g) microdiscs, h) fully abraded, i) edge abrasion, j) percussive
926 marks

927 Figure 4. Cathodoluminescence and UV luminescence optical responses.

928 Figure 5. Nitrogen aggregation of Guyana's diamonds. a) Total N (ppm) vs N_B (%) plot of
929 abraded and non-abraded diamonds (Total N \pm 24 ppm, % N_B \pm 1.7%), b) nitrogen
930 aggregation type classification, c) representative FTIR spectrum showing carbon and
931 nitrogen in diamond regions.

932 Figure 6. $\delta^{13}C$ values (in ‰_{VPDB-LSVEC}) of Guyana's diamonds compared to other South
933 American diamonds. (¹Tappert et al. 2006; ²Kaminsky et al 2000; ³Smith et al. 2016)

934 Figure 7. Ca# vs Mg# plot of mantle and crustal derived accessory garnets (Schulze et al. 2003).

935 Figure 8. Comparative detrital zircon U-Pb age distributions from alluvial and colluvial samples
936 at Kurupung.

937 **Supplementary figure captions**

938 Figure A1. Kernel density plot of N (ppm) between a) abraded and b) non-abraded diamonds,
939 and c) Bayesian Information Criteria vs component plot showing a 21 component mixture
940 as the most appropriate number of nitrogen populations of the FMM.

941 Figure A2. Detrital zircon U-Pb age distributions plotted as a) cumulative and b) relative
942 probability density plots (Sharman et al. 2018). Vertical grey bar indicates the
943 depositional age range of the Roraima Supergroup. Peak ages are labeled.

944 **Table captions**

945 Table 1. Summary morphology.

946 Table 2. Pit dissolution textures of Guyana's diamonds.

947 Table 3. Optical spectroscopy.

948 Table 4. Spectroscopic comparisons between abraded and non-abraded diamonds.

949 Table 5. Guyana diamond inclusion types.

950 Table 6. Nitrogen concentrations of Guiana Shield diamonds.

951 Table 7. Formation temperatures of Guiana Shield diamonds.

952 **Supplementary table captions**

953 Table A1. Abraded vs non-abraded diamond comparisons.

954 Table A2. Comparative FTIR and $\delta^{13}\text{C}$ of Guyana's diamonds.

955 Table A3. Comparative FTIR derived N concentrations, residence temperatures, CL, and UV
956 responses for Guyana's diamonds.

957 Table A4. Accessory mineral compositions (wt%).

958 Table A5. U-Th-Pb ages of detrital zircons from diamondiferous alluvium and colluvium
959 analyzed at the University of Arkansas.

960 **End**

Figure 1

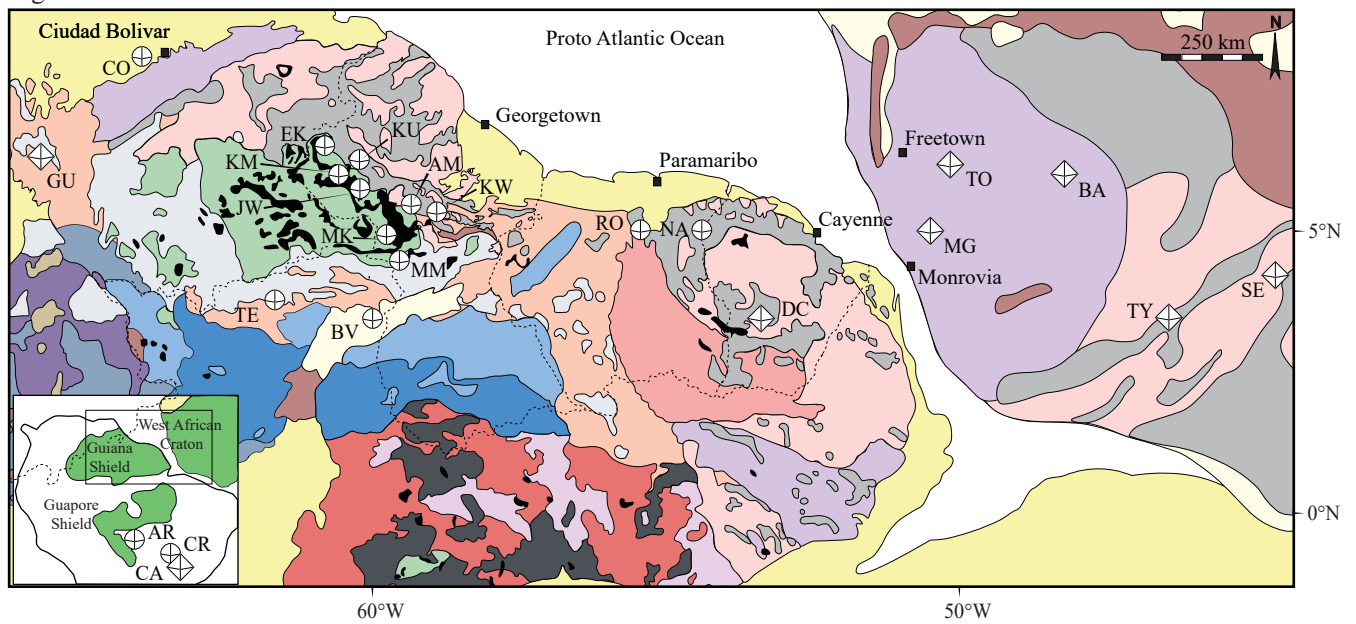


Figure 1 - Legend

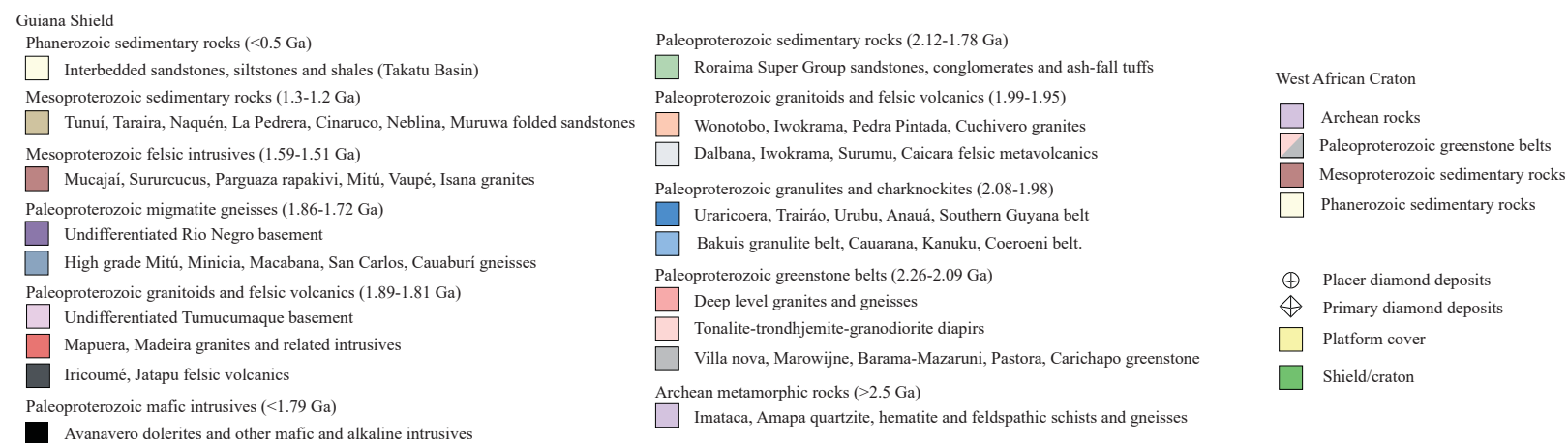


Figure 2

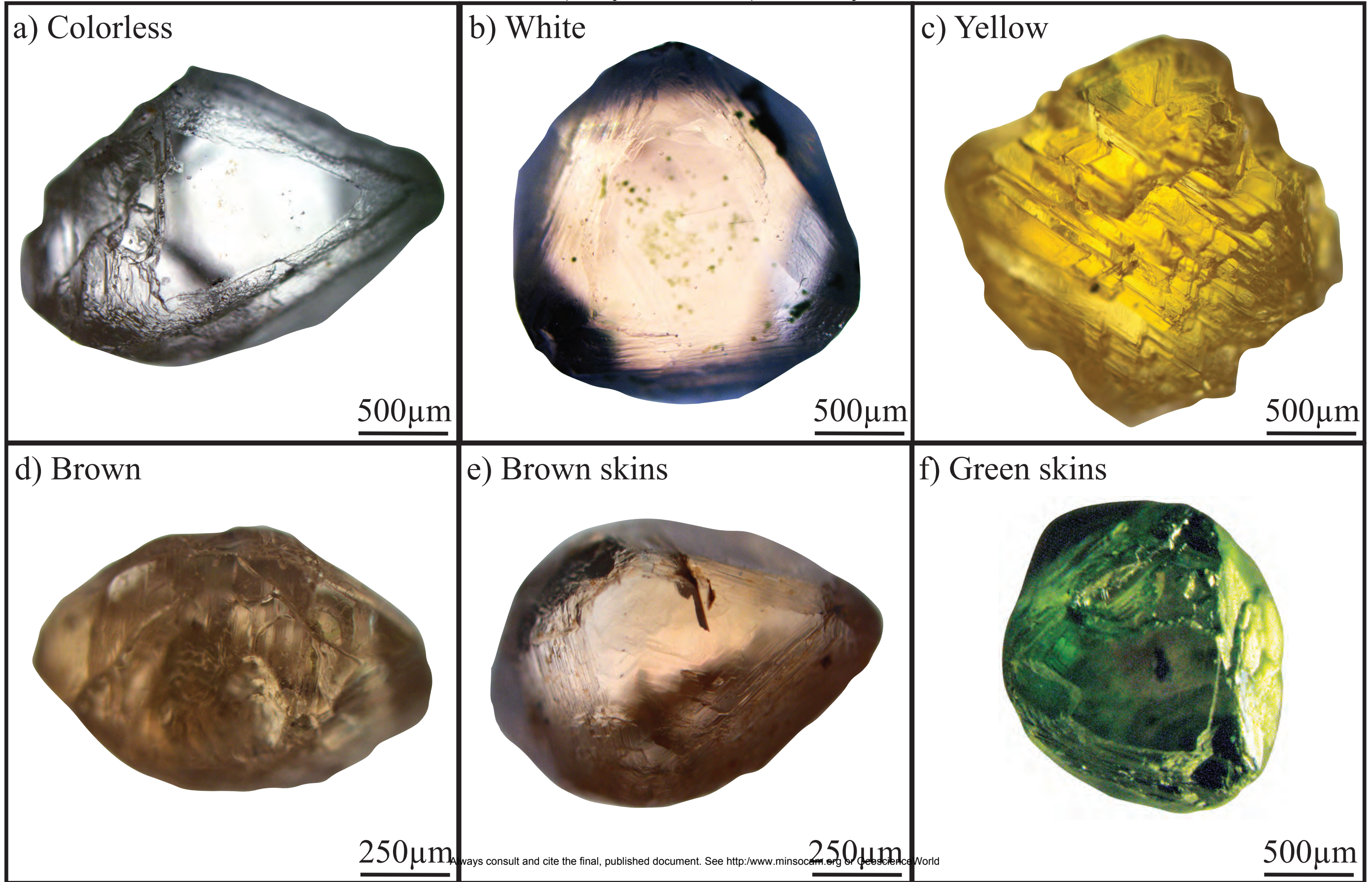
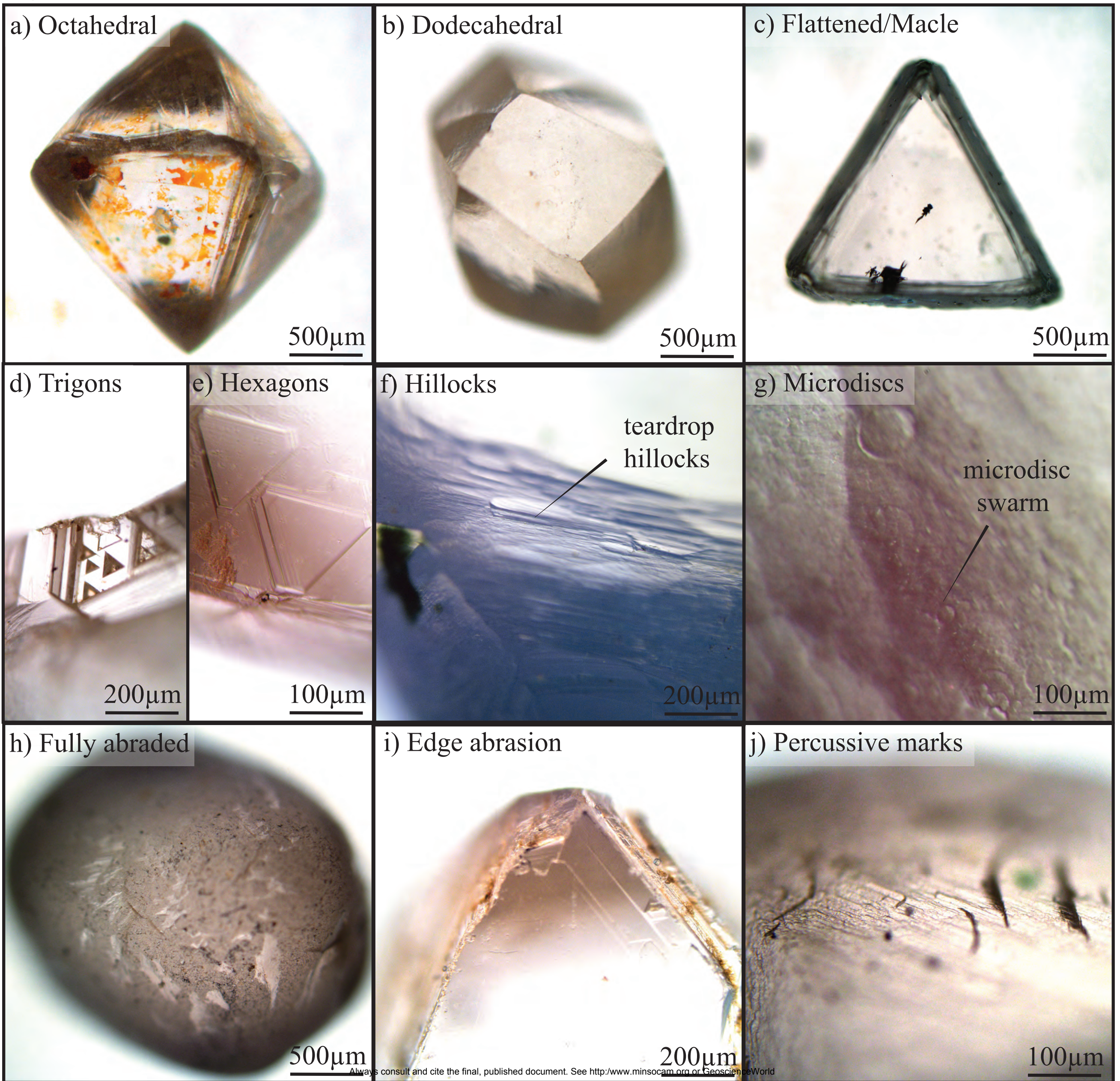


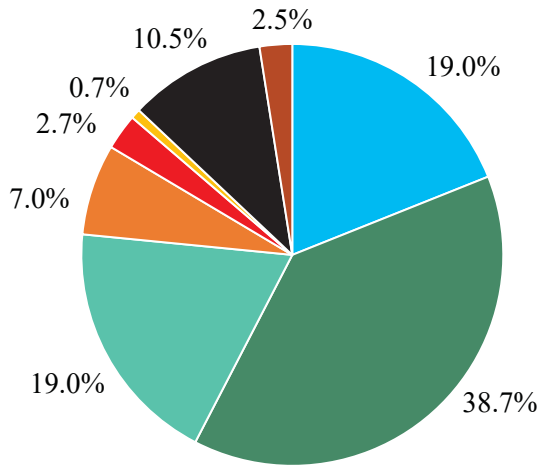
Figure 3



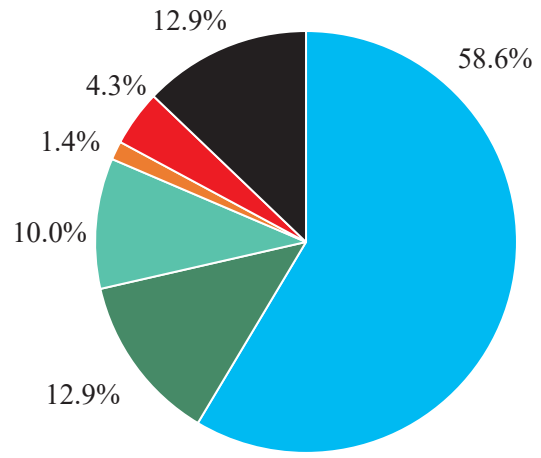
a) Cathodoluminescence response

■ No Response ■ Green ■ Orange ■ Yellow ■ Blue ■ Turquoise ■ Red ■ Combination

Abraded



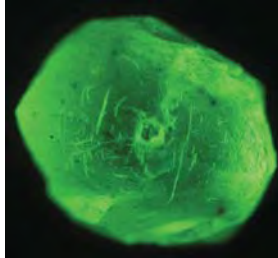
Non-abraded



Blue



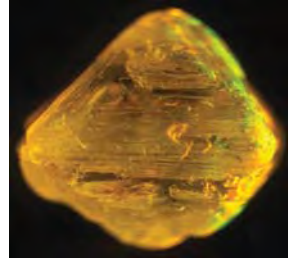
Green



Turquoise



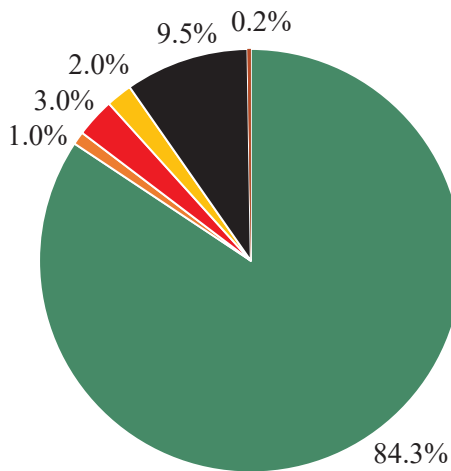
Yellow



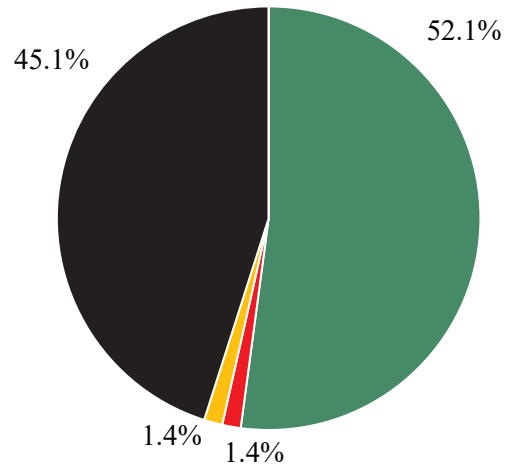
b) UV luminescence response

■ No Response ■ Green ■ Orange ■ Yellow ■ Red ■ Combination

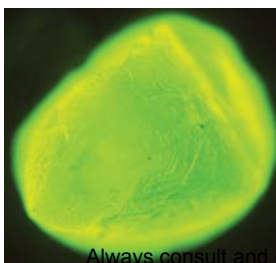
Abraded



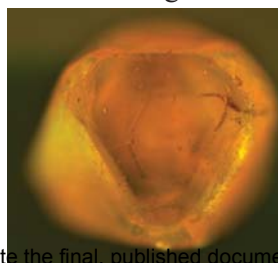
Non-abraded



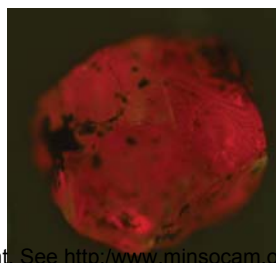
Green



Orange



Red



Yellow

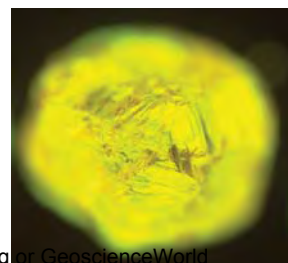


Figure 5

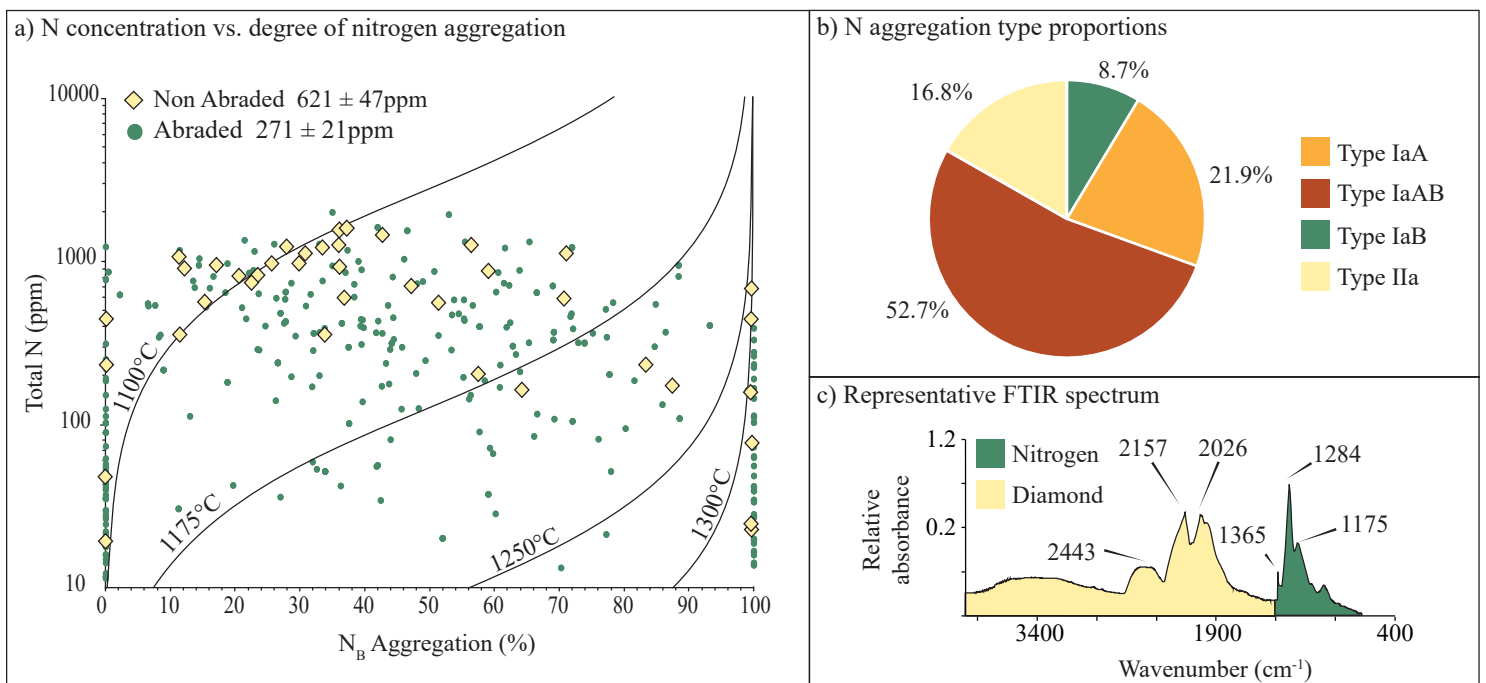


Figure 6

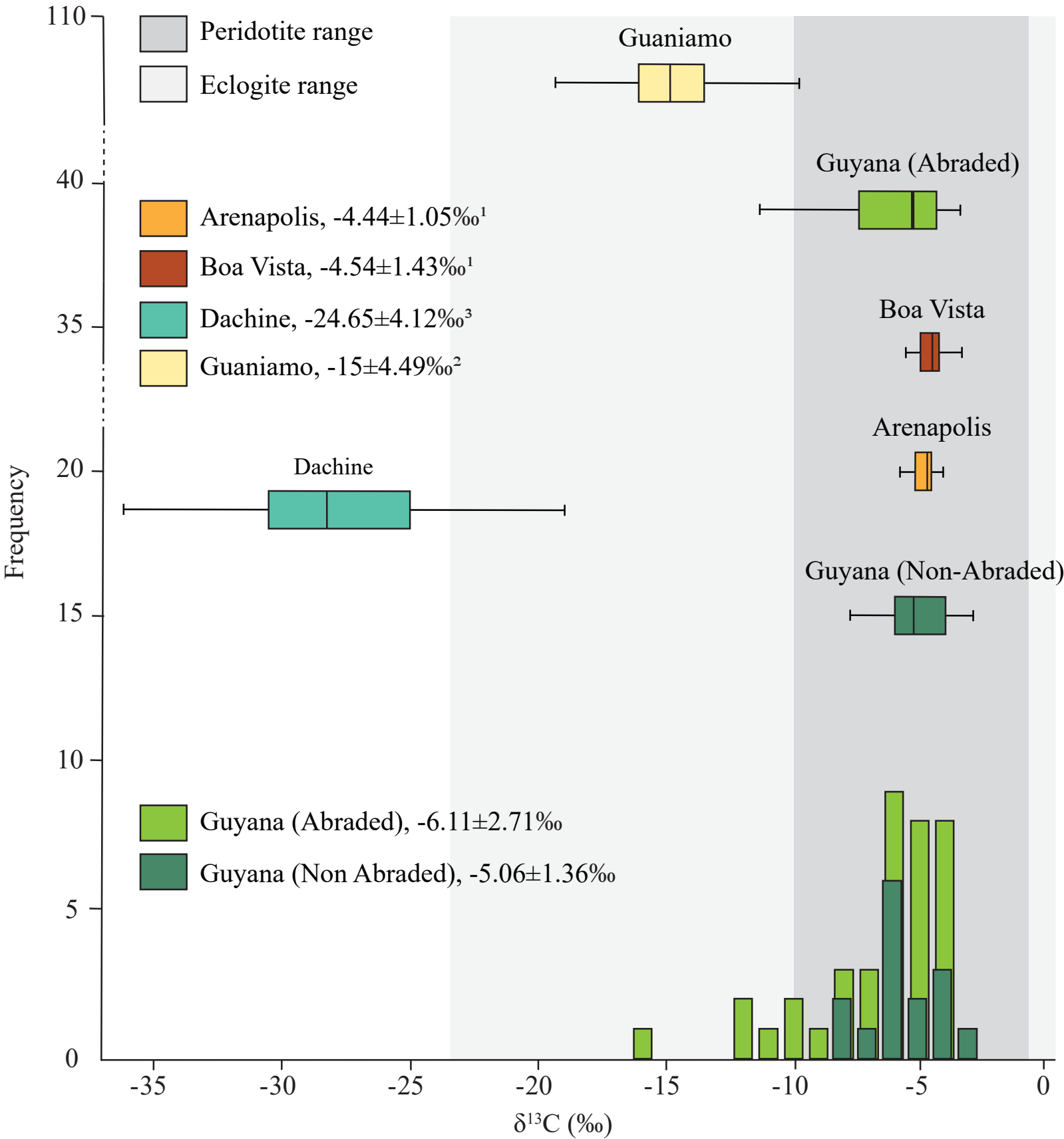


Figure 7

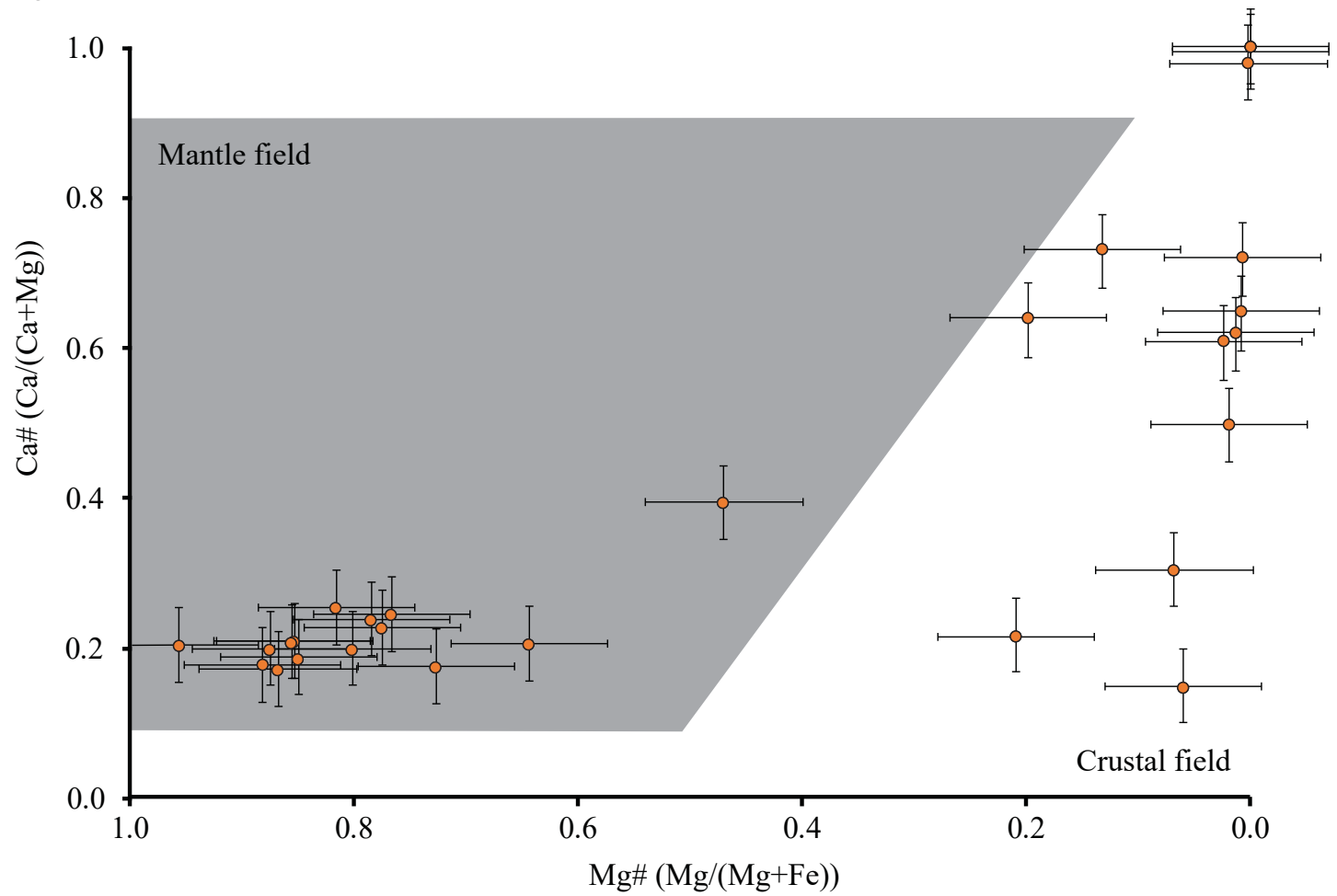


Figure 8

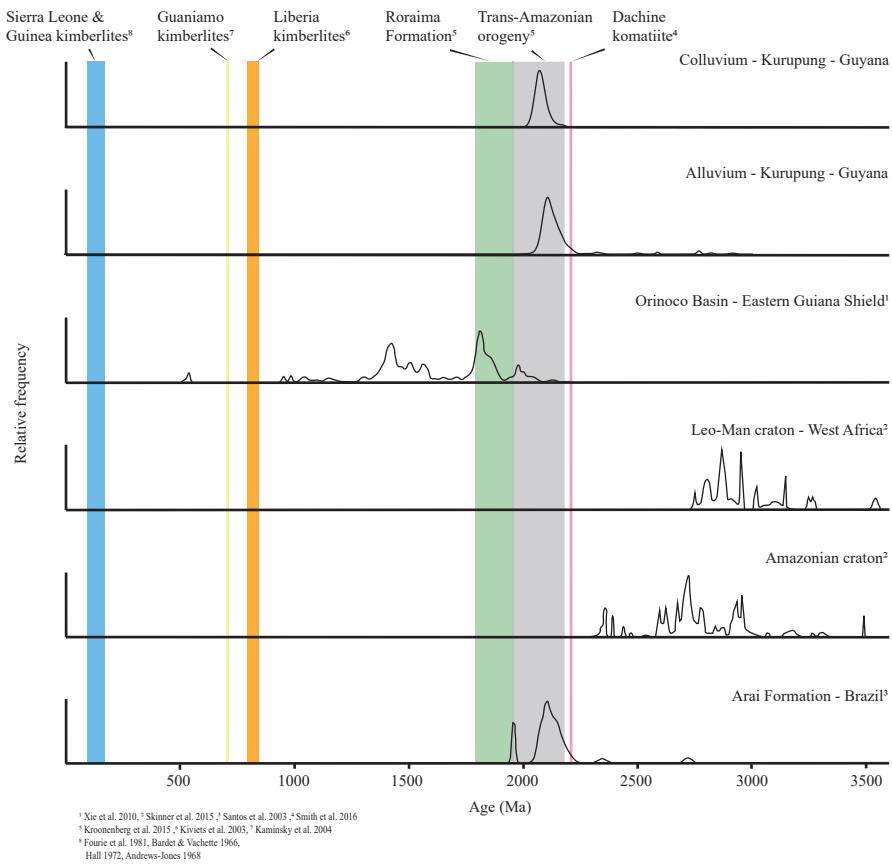


Table 1. Summary morphology

Location	<i>n</i>	Color							Habit					Spotting				Late Stage Etching		Sedimentological abrasion		
		B	Br	Y	Gr	P	W	X	O	D	Co	C	Fl	Unk	Gr	Br	Co	X	Etching	No Etching	Abraded	Non Abraded
Ekereku	226	0	9	6	0	0	0	211	69	103	29	9	11	5	97	9	18	205	90	208	159	53
Jawalla	19	0	1	2	0	0	0	16	6	7	4	1	1	0	8	0	0	11	6	13	19	0
Kamarang	154	0	6	2	0	0	1	145	44	16	35	0	40	19	95	4	9	46	53	101	140	13
Konawaruk	6	0	0	0	0	0	0	6	3	1	0	0	2	0	3	0	1	2	0	5	6	0
Kurupung	81	0	1	4	0	0	1	75	25	17	11	3	18	8	30	2	6	90	28	55	78	5
Maikwak	3	0	0	0	0	0	1	2	1	2	0	0	0	0	3	0	0	0	0	3	3	0
Monkey Mt.	3	0	0	0	0	0	0	3	2	1	0	0	0	0	2	0	0	1	0	3	3	0
%		0.0	3.5	2.8	0.0	0.0	0.6	92.7	30.4	29.8	16.0	2.6	14.6	6.5	37.1	2.3	5.3	55.3	31.3	68.7	85.2	14.8

B - blue, Br - brown, Y - yellow, P - pink, W - White, X - no colour/spotting

O - octahedral, D - dodecahedral, Co - combination, C - cubic, Fl - flattened/elongate, Unk - unknown

Table 2. Pit dissolution textures of Guyana's diamonds

Type	Trigons	Tetragons	Hexagons	Trapezoids
Point Bottom (%)				
very fine (< 25 μm)	7.7	1.3	0.0	0.0
fine (25 - 50 μm)	2.6	3.8	0.0	0.0
medium (50 - 75 μm)	1.3	5.1	1.3	0.0
coarse (75 - 100 μm)	0.0	6.4	0.0	0.0
very coarse (> 100 μm)	0.0	1.3	0.0	0.0
Total %	11.5	17.9	1.3	0.0
Flat Bottom (%)				
very fine (< 25 μm)	5.1	0.0	5.1	0.0
fine (25 - 50 μm)	14.1	0.0	9.0	5.1
medium (50 - 75 μm)	5.1	0.0	1.3	1.3
coarse (75 - 100 μm)	11.5	3.8	3.8	0.0
very coarse (> 100 μm)	1.3	0.0	1.3	1.3
Total %	37.2	3.8	20.5	7.7

error $\pm 5 \mu\text{m}$, # of diamonds - 370, # of diamonds with dissolution pits - 78

Table 3. Optical spectroscopy

Location	Cathodoluminescence								UV fluorescence						<i>n</i>
	B	Gr	T	O	R	Y	X	Z	Gr	O	R	Y	X	Z	
Ekereku	80	53	32	9	3	1	28	2	154	1	3	1	50	0	209
Jawalla	3	4	7	4	0	0	0	1	18	1	0	0	0	0	19
Kamarang	20	66	26	12	5	1	19	3	127	0	7	5	13	1	152
Konawaruk	1	3	1	0	0	0	1	0	6	0	0	0	0	0	6
Kurupung	10	36	16	4	6	1	3	4	65	2	3	3	7	0	80
Maikwak	1	2	0	0	0	0	0	0	3	0	0	0	0	0	3
Monkey Mt.	2	0	1	0	0	0	0	0	3	0	0	0	0	0	3
%	24.8	34.8	17.6	6.2	3.0	0.6	10.8	2.1	79.5	0.8	2.7	1.9	14.8	0.2	

Cathodoluminescence, n - 471, UV fluorescence, n - 473

B - blue, Gr - green, T - turquoise, Y - yellow, O - orange, R - red, X - no response, Z - combination

Table 4. Spectroscopic comparisons between abraded and non-abraded diamonds

Spectroscopy	Abraded		Non-abraded	
FTIR¹	N (ppm)	<i>n</i>	N (ppm)	<i>n</i>
mean	271 ± 21	349	621 ± 47	44
median	109		590	
σ	353		473	
skewness	1.82		0.26	
kurtosis	6.62		1.91	
FMM populations				
Pop. 1	1911 ± 150	2	—	—
Pop. 2	1234 ± 99	16	—	—
Pop. 3	—	—	968 ± 79	18
Pop. 4	610 ± 52	54	604 ± 48	7
Pop. 5	351 ± 29	60	390 ± 26	4
Pop. 6	193 ± 16	30	180 ± 16	6
Pop. 7	84 ± 8	34	—	—
Pop. 8	39 ± 3	46	47 ± 3	1
Pop. 9	21 ± 2	26	23 ± 1	4
Pop. 10	13 ± 1	16	—	—
Pop. 11	6 ± 0.4	5	4 ± 0.3	2
Cathodoluminescence²				
	%	<i>n</i>	%	<i>n</i>
Blue	19.0	76	58.6	41
Green	38.7	155	12.9	9
Turquoise	19.0	76	10.0	7
Orange	7.0	28	1.4	1
Red	2.7	11	4.3	3
Yellow	0.7	3	—	—
No Response	10.5	42	12.9	9
Combination	2.5	10	—	—
UV luminescence				
	%	<i>n</i>	%	<i>n</i>
Blue	—	—	—	—
Green	84.3	339	52.1	37
Turquoise	—	—	—	—
Orange	1.0	4	—	—
Red	3.0	12	1.4	1
Yellow	2.0	8	1.4	1
No Response	9.5	38	45.1	32
Combination	0.2	1	—	—

¹ Abraded vs Non-abraded log N (ppm), |t|-test statistic: 12.7 > |t|-threshold value: 1.3, with 95% compatibility interval and p < .00001

² Abraded vs Non-abraded CL (%), χ²- test statistic: 287 > χ²-threshold value: 14.1, with 7 degrees of freedom, a 90% compatibility interval, and p < .00001

Table 5. Guyana diamond inclusion types

Inclusion	# of diamonds	Paragenesis
Chromite	11	Peridotitic
Enstatite ¹	15	Peridotitic
Forsterite ²	42	Peridotitic
Cr-pyrope garnet	3	Peridotitic
Almandine garnet	1	Eclogitic
Coesite	1	Eclogitic
Clinopyroxene	1	Eclogitic
Rutile	15	Eclogitic

¹Raman spectra doublet peaks indicate a more Mg rich and enstatite composition. ²Raman spectra doublet peak and lower intensity of ν_3 mode peak suggest a more forsteritic composition (Mg# ~ 90)

Table 6. Nitrogen concentrations of Guiana Shield diamonds

Location	Total N \pm σ (ppm)	%N _B	n
Guyana			
Ekereku	407 \pm 472	38 \pm 34	134
Jawalla	123 \pm 201	27 \pm 34	19
Kamarang	275 \pm 310	38 \pm 34	150
Kurupung	242 \pm 352	36 \pm 41	79
Konawaruk	249 \pm 265	18 \pm 19	6
Maikwak	250 \pm 78	34 \pm 5	3
Monkey Mt.	610 \pm 138	65 \pm 16	3
Venezuela			
Los Coquitos ¹	641 \pm 324	62 \pm 19	77
Guaniamo ²	620	69	192
French Guiana			
Dachine ³	20 \pm 29	NA	18
Brazil			
Boa Vista ⁴	345 \pm 412	39 \pm 30	34

¹ Kaminsky et al 2006, ² Kaminsky et al 2000, ³ Smith et al 2016, ⁴ Kaminsky et al 2001, ⁴ Tappert et al 2006

Table 7. Formation temperatures of Guiana Shield diamonds

Location	T (°C)	n	Derivation
Guyana			
Abraded	1128 ± 104	208	N aggregation (1.3Ga residence)
Non-abraded	1101 ± 72	34	N aggregation (2.6Ga residence)
mean	1124 ± 100	242	
median	1148	242	
skewness	-1.49	242	
kurtosis	1.72	242	
Brazil¹			
Boa Vista	1208 ± 74	27	Chromite-Olivine inclusion equilibration
Venezuela²			
Guaniamo	1116 ± 99	6	Garnet-Diopside inclusion equilibration

¹Tappert et al 2006, ²Kaminsky et al 2000